(Langmuir)

Elucidating Molecular Interactions in Glycerol Adsorption at the Metal-Water Interface with Density Functional Theory

Nannan Shan[a], *Bin Liu*[a,*]

[a]Department of Chemical Engineering, Kansas State University, Manhattan, KS 66506, United States

Corresponding Author
*E-mail: binliu@ksu.edu

ABSTRACT

Glycerol is an extremely versatile platform molecule for chemicals and fuels production, as evidenced by successful demonstrations in electrochemical and thermochemical processes, where key catalytic chemistries occur at the solid-liquid interface. Despite the remarkable progress to enrich the first-principles-based computational toolset to reveal and characterize solvent structures in the past decade, techniques for realistic and efficient molecular-level modeling to study aqueous phase glycerol chemistry are still far from mature. Many aqueous phase catalytic systems are deemed too complex for routine modeling because of the highly correlated structures at the heterogeneous solid-liquid interface. This article merges recent developments in quantum mechanical solvation models and oxygenated hydrocarbon conversion chemistry by revisiting the molecular interactions of adsorbed glycerol and its dehydrogenation intermediates at the water-metal interface. Explicit participation of water through the establishment of water-adsorbate, water-water, and water-metal interactions on Pt(111) was investigated using density functional theory. In periodic models, the adsorption favors network-like structures with adsorbates as nodal points linked by co-adsorbed water molecules. We also showed that such these adsorption patterns actually preserve the original bond-order-based scaling relationship framework established without the consideration of solvent. This behavior can be exploited to improve computational efficiency for future analysis of catalytic polyol conversions in the aqueous phase environment.

INTRODUCTION

Driven by the quest for sustainable fuels and chemicals, biomass-derived glycerol,[1-5] furanic compounds[6-8] are listed as key platform compounds. Glycerol, a C3 polyol consisting of three hydroxyl groups, exhibits an extremely versatile utility.[9,10] Boosted by the biodiesel production, glycerol production has nearly doubled during the period of 2001-2011,[11] and is expected to quadruple by 2025.[12] The economic appeal strengthens glycerol's position as an affordable feedstock for the conversion into value-added marketable commodities.[12] Recent reviews have shown that[2,9,10] hydrogen, propanediols (PDOs), glyceraldehyde, dihydroxyacetone, alcohols, and organic acids can be derived from catalytic transformations of glycerol.[2, 9-10]

Aqueous phase reforming (APR) of glycerol has been demonstrated successfully to be a viable route for hydrogen production at 498 – 543 K and 25 – 50 bar, as schematically illustrated in Figure 1.[13] Using platinum as the catalyst, promising hydrogen yield (~68%)[14] and selectivity (up to ~75%)[13] have been achieved. Over Pt, cleavage of glycerol C–H, O–H, and C–C bonds, leading to the formation of hydrogen and CO or CO_2 (if coupled with water-gas shift reaction), are promoted, while routes involving C–O bond cleavage (producing alcohols and alkanes) are effectively suppressed at the same time.[15,16] On the other hand, the C–O bond cleavage is promoted on Rh[17] and Ru[18], over which hydrogenolysis becomes the pre-dominant route at 80 bar and 473 K. As more attention is given to non-platinum group metals (such as Ni[19]) and platinum-based alloys (Pt-Ni,[20] Pt-Mo,[21,22] Pt-Re[23]) in recent years, mechanistic understanding becomes necessary and even crucial in the assessment catalyst behavior, and more importantly, in the formulation of rational catalyst development principles.[24]

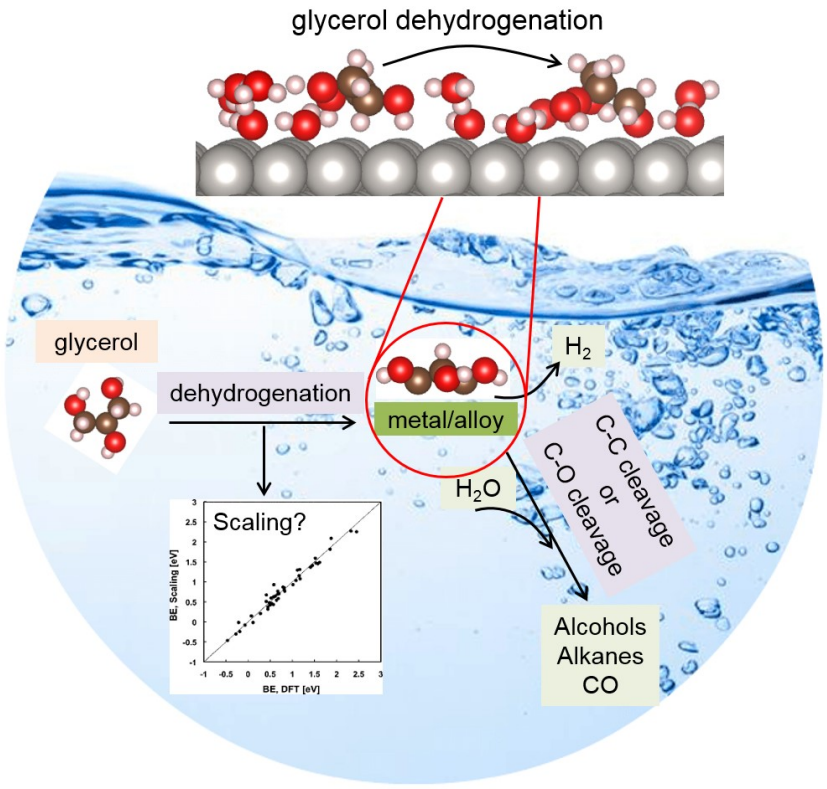

Figure 1. Glycerol conversions to chemicals on transition metals in aqueous phase. Inset scaling figure was adapted with permission from Ref. [15].[15] Copyright [2011] {American Chemical Society}.

On most catalysts, glycerol conversion proceeds via parallel reaction pathways (dehydrogenation, hydrogenolysis, or oxidation) that are interwoven.[9] Despite a high level of mechanistic complexity, the identified pathways derived from independent quantum mechanical studies over well-defined catalytic systems are in satisfactory agreements with experimental observations, by using relatively simple models, for instance, with uniform low-index single crystal active sites in an idealized reaction environment.[15-17,25-29]

Glycerol is processed in the aqueous phase on a much more regular basis, especially for APR and hydrogenolysis, at temperatures above 450 K and pressures greater than 25 bar.[9] Hence, water is intricately involved as a medium for both reactants and products in the aqueous phase,

as well as the intermediates on catalyst surfaces. Specifically, for catalytic reactions, the participating water is capable of modifying both reaction energetics and transition state energies in oxygen reduction reaction (ORR),[30,31] NH_3 synthesis,[32] electrochemical CO_2 reduction,[33-35] and so on. For oxygenated hydrocarbons, Zope et al.[36], showed that ethanol oxidation on gold actually utilizes hydroxide ions generated from OOH in aqueous solutions rather than molecular oxygen directly using isotopic $^{18}O_2$ and $H_2{}^{18}O$ probes.

Gaining molecular insights into the structure at the interface of aqueous solution and metal surface can be greatly aided by the improvement of interfacial structure descriptions, modeling technique integration, and interatomic potentials. At the quantum mechanical level, through either ab initio molecular dynamics or density functional theory (DFT) calculations, the sophistication and accuracy for the modeling of water-solid interfaces have reached an unprecedented level.[37] In this article, relevant theoretical developments and impact will be discussed in the following section. As can be seen, the literature survey has exposed that acquiring a full molecular perspective on the catalysis associated with glycerol remains extremely challenging because: (1) first-hand information on molecular interactions between adsorbate, solvent, and substrate for the construction of representative models is very scarce; and (2) the inevitability model sizes are too large for standard first-principles modeling.

Glycerol and most of its derivatives on many metallic APR catalysts in solvent-free systems are shown to follow empirical formulations derived from approximate bond-order conservation concepts, known as the scaling relationship, which is shown that such an relationship can be exploited as a reliable screening tool in the place of DFT calculations.[15,16,24,25] Driven by the establishment of a similar scaling relationship for these adsorbates in a solvated environment, periodic DFT calculations have been employed to reveal patterns described in terms of various

water-adsorbate, water-metal, and water-water interactions on well-defined metal-liquid interfaces, which can be considered as a step toward qualitative and quantitative descriptions of catalytic conversions of oxygenated hydrocarbon species in the aqueous phase.

SOLVATION MODELS BASED ON QUANTUM MECHANICAL THEORIES

Implicit solvation models

In implicit solvation models, solute molecules in the dielectric medium are commonly treated as being immersed in a 'solvent cavity'. If the continuum dielectric medium is considered as an isotropic, the implicit solvation method is an appealing approach to lower the computational cost by reducing the total degrees of freedom of the system.[38,39] The electrostatic contribution to the overall solvation free energy can be obtained numerically by discretizing the Poisson differential operator. In the implementation of implicit solvation models, care has to be taken in the selection of the cavity shape and size, which should be able to reproduce the shape of the solute molecule to minimize distortions of the solvation field: too large cavities will dampen the solvation effects, while too small cavity may result in errors in interaction energy calculations at the solute-solvent interface. Comprehensive reviews of implicit solvation methods, including the rule to determine appropriate cavity, are presented by Tomasi, Cramer, and their coworkers.[38,39] The so-called conductor-like screening model (a.k.a COSMO[40]) is a close family to the popular polarizable continuum model (PCM),[38] and has been successfully integrated into commercial softwares such as ADF.[41] To account for non-electrostatic effects, COSMO for real solvents (i.e., COSMO-RS) has been recently developed to compute solvation free energies of neutral solutes.

In an implicit solvation setting, Jeong et al.[42] obtained the conformational preference of glycerol at the M06-2Z/cc-pvtz level of theory in aqueous phase. It is shown that, glycerol exists

as an ensemble of many feasible configurations due to the weakened intramolecular hydrogen bonding. This is a contrast to the glycerol's gas phase configuration, in which glycerol strongly prefers the existence of an intramolecular hydrogen bonding between two terminal hydroxyl groups.[15]

An implicit solvation scheme compatible to the Kohn-Sham framework was introduced by Fattebert and Gygi,[43,44] where the electrostatic energy term in the Hohenberg-Kohn formulation is revised using solution of the Poisson equation. Theory such as JDFT by Arias et al.[45] has been developed to study solid surfaces in solution. Hennig and coworkers[46,47] implemented a self-consistent scheme, as in VASPsol, to account for both electrostatic and non-electrostatic (e.g., dispersion) effects on extended and discrete solid-liquid interface. Most recently, Garcia-Ratés and López[48] succeeded in developing a multigrid continuum model (i.e., MGCM), implemented in the Vienna *ab initio* Simulation Package (VASP), to compute the energetics of adsorbed water, methanol) in solutions. With the newly developed MGCM, it is shown that the trend for methanol and water adsorption on Pt(111) can be reversed whether or not the implicit solvation is included.[48] Given the available methods for implicit solvation treatments, Deskins et al.[49] studied the adsorption of 41 species (i.e., C, O, S, N, CH_x, NH_x, etc.) on Pt(111) using three implicit models (i.e., VASPsol, JDFTx, and COSMO), and found that the absolute solvation energy values indeed vary. However, the relative solvation effect remains consistent. Despite the computational advantages, the description of the structural and dynamic properties of a solvated system might be inadequate due to the inherent treatment of the solvent in implicit solvation models. In many catalytic processes, the liquid phase is more than just a dielectric continuum background, as solvent molecules in the liquid phase often participate in chemical reactions.

Explicit solvation models for solid-water interfaces

Explicit solvation models describing adsorbed molecular species on solid surfaces, emerged in an aqueous solution, require that the simulation box be filled with water molecules. At the quantum mechanical level, the computational cost is prohibitive if the aqueous phase is realistically represented. Solute-solvent interactions are often limited to within one solvation shell, resulting in a large portion of computing resource actually spent on computing the degrees of freedoms associated with solvent-solvent interactions in the bulk solution. Thus, hybrid solvation models, blending the implicit treatments to account for interactions indirectly contributing to solute or adsorbate properties in the aqueous phase, should in principle be an effective way to improve computational efficiency. The schematic representation of the adsorption of an immersed adsorbate (denoted as $E_{ads(aq)}$) on a metal surface is illustrated in Figure 2, where water-adsorbate, water-water, and water-metal interactions are explicitly indicated at the metal-water interface.

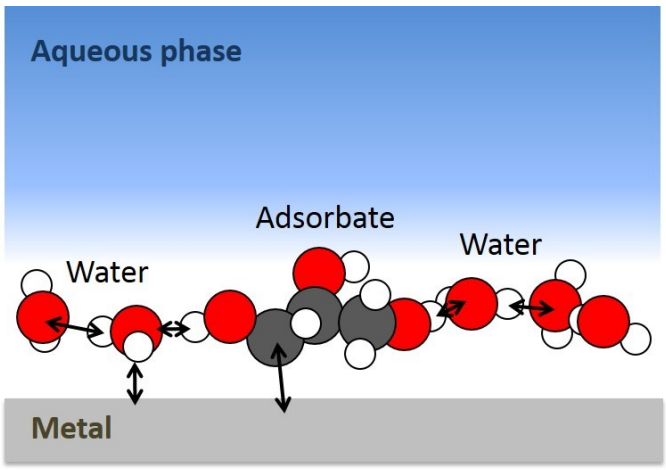

$$E_{ads(aq)} = E_{ads\text{-}metal} + E_{ads\text{-}water} + E_{water\text{-}water} + E_{water\text{-}metal}$$

Figure 2. Schematic illustration of contributions to adsorptions at the water-metal interface.

All-atom molecular dynamics simulations with classical force field potentials (e.g., SPC, TIP3P, TIP4P) has been playing an influential role in producing structural and thermodynamic properties of explicit aqueous phase systems.[50] Unfortunately, there are stiff challenges to adapt for chemical processes involving heterogeneous water-metal interfaces due to the lack of reliable force fields that are readily available. *Ab initio* molecular dynamics (e.g., the Car-Parrinello approach[51]) does provide a gateway by removing the dependence on intermolecular potentials at the expense of computing power to achieve statistically meaningful molecular information.

At the interface where catalysis occurs, the principle is that detailed attention should be given to molecular interactions directly responsible for bond cleavage/formation or charge transfer, as illustrated in Figure 2. Ice-like water bilayer models covering metal slabs are regarded representative to mimic the water-metal interface for periodic DFT calculations. To a great extent, the rationale behind such models can be traced back to surface science studies of water structures on solid surfaces. Over thirty year ago, work by Thiel and Madey[52] revealed that the water structure on metal can be described as a 'buckled' bilayer arranged as hexagons with half of the water molecules bind directly on the surface. Aided by XPS and XAS, Ogasawara et al.[53] reported a flat water bilayer on Pt(111). Absorption spectroscopy obtained at low temperature (e.g., 84 K) further showed that water binds on Pt through the oxygen lone pair. The strong lateral interaction through hydrogen bonding is a main mechanism responsible for water clustering.[54] In Carrasco and Michaelides' recent review,[55] high-resolution experimental STM and DFT calculations are considered a powerful combination to gain molecular insights into behaviors of water clusters (including monomer, dimer, trimer, tetramer, and hexamer), as well as 1-D, 2-D, and 3-D water networks on the surface. With the access to atomic-scale resolution measurements on well-defined surfaces, it becomes possible to build representative molecular

models for fundamental studies, which then paves the way for more sophisticated modeling.

Recently, the early bilayer theory is being challenged as the water overlayer configurations are shown to be diverse. Over Pt(111), configurations with mixed pentagonal, hexagonal, and heptagonal water rings have been observed with STM, and later confirmed by DFT calculations.[56,57]

The wetting behavior is another indicator of the interaction between water overlayer and metal surfaces. On Pt, adsorbed water molecules remain largely intact. On the other hand, water dissociation is known to occur on Ru(0001).[58] On Cu(110), 2-D water structure is also shown to consist of hydroxyl groups from partial dissociation of water, at a molar ratio of H_2O:OH = 2:1.[59]

Schnur and Groß[60] showed that the presence of metal substrates add substantial polarization on the water overlayer. In addition, some metastable states of the overlayer are energetically stabilized. As shown by Neurock and coworkers,[37] it takes 0.16 – 0.3 eV for water bilayer to overcome the energy barrier to switch from the 'up' orientation to the 'down' orientation.

The ordered water overlayer above the metal surface can be perturbed by adsorbates. For instance, with pre-adsorbed H atoms on Pt(111), it has been shown that the water bilayer moves away from the surface.[60] Also, a greater order has been predicted, especially when compared to the overlayer directly above Pt(111) without the pre-adsorbed hydrogen atoms. This observation indicates that, near the water-metal interface, solvent structures are influenced by competing water–water and water-metal interactions.

Understanding the influence of water on physi- or chemi-sorption is one key focus in the modeling of aqueous-phase catalytic processes. On bimetallic Pt-Ru (111), Desai and Neurock[61] pointed out that although the active site (Ru) responsible for water dissociation is unaffected without the inclusion of explicit solvent molecules, the dissociation step becomes more

energetically favorable (0.27 eV) compared to that without the presence of accompanying water molecules (0.55 eV). This suggests that the product state, i.e., dissociated H and OH, is stabilized to a greater extent than the reactant state. Moreover, the transition-state complex structure can also be stabilized as the activation energy is lowered from 1.09 eV in the vapor phase to 0.28 eV.

Extended analysis from the stabilization of a single elementary state to the entire reaction pathway would provide a more faithful description of the thermodynamic landscape in the solvated environment. Take CO_2 electroreduction as an example, Peterson and co-workers have proposed that, in the solvent-free environment, the formation of formyl group (CHO), rather than COH, is the electrochemical potential limiting step for CH_4 production.[62-64] With a water bilayer model, Shi and Nørskov,[65] again, showed that CHO is more stable than COH, which is independently confirmed by Jónsson and Skúlason.[66,67] However, the energy barrier for CHO formation via CO protonation in the water-assisted H shuttling mechanism, supported by the explicit solvent model, is higher.[34,68] Also, in water-assisted H shuttling, it is found that the O-H bond formation barrier, as in CO-to-COH, is noticeably lowered.[34]

Because a specific geometric orientation facilitating proton transfer is required, implicit solvation models can be inadequate. For instance, molecular modeling of reactions involving proton-coupled electron transfer (PCET) steps in hydrogen evolution,[69] hydrogen oxidation,[70] protonation necessitates explicit solvation modeling. To further reduce the cost of computation required by explicit solvation modeling, models describing solvation effect using few water molecules in direct contact with adsorbates have been suggested.[34,71,72] Sautet et al.[73] pointed out that the intramolecular hydrogen bonds within the carbon skeleton and intermolecular hydrogen bond formed between water-adsorbate can modulate the reactivity of O-H or C-O bond dissociations for adsorbed alcohols.

The extent of solvation based on the use of a finite number of water molecules has to be verified. Based on methanol adsorption, Garcia-Ratés et al.[74] identified different roles of water molecules surrounding methanol. The water molecule in direct coordination with the hydroxyl group provides the main source of stabilization of adsorbed alcohol, however, such coordination could also limit the binding of the hydroxyl group to the surface. For water molecules away from the hydroxyl group, there is a residual effect on the decomposition pathway of methanol. As a tradeoff, Garcia-Ratés et al.[74] proposed a hybrid model that contains two water molecules explicitly coordinating with the adsorbed methanol, and further increase of the number of water molecules will not improve the model. Solvent elsewhere can be treated as a continuum medium using MGCM discussed in the previous section (as illustrated in Figure 2).[48]

ACCELERATED SCREENING BY LINEAR SCALING RELATIONSHIP

In order to decipher the chemistries for glycerol conversion, the ability to identify key intermediates associated with respective dehydrogenation, hydrogenolysis, or oxidation pathways efficiently is crucial.[9] Modeling of catalytic conversion of glycerol using first-principles is already challenged by the large number of reaction intermediates in a pool of 80 species: an estimation based on dehydrogenation chemistry alone.[15]

In the past few years, the adsorption patterns of chemisorbed glycerol ($C_3H_8O_3$) and its various dehydrogenenation intermediates on several transition metal and metal alloys have been studied using periodic DFT calculations.[15,16] Other oxygenated hydrocarbons, for which this rule is also applicable, include methanol (CH_3OH), ethylene glycol (a C2 polyol), and erythritol (a C4 polyol), as well as intermediates from various C-H and O-H bond scissions. The structures of mono-dehydrogenated intermediates ($C_3H_7O_3$, i.e., glycerol minus one hydrogen atom), as well

as glyceraldehyde, and dihydroxyacetone (the two di-dehydrogenated products) on Pt(111), are illustrated in Figure 3(a).

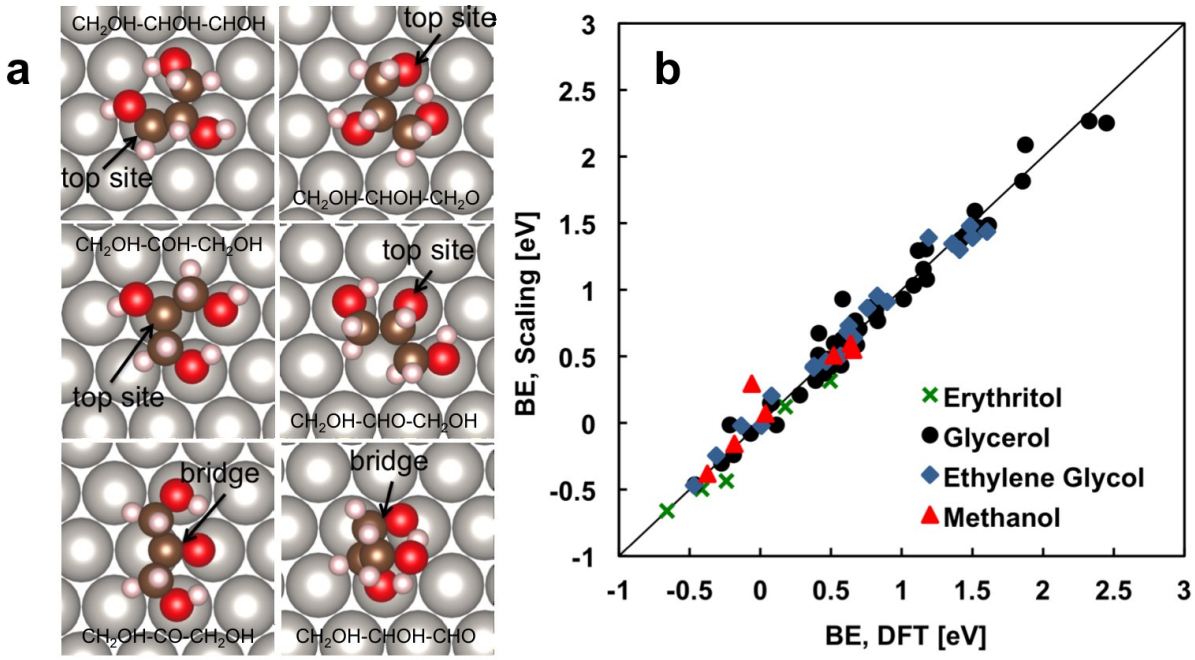

Figure 3. (a) Adsorption configurations of selected glycerol dehydrogenation intermediates on Pt(111) from periodic DFT calculations. C, O, H, and Pt are depicted in brown, red, pink, and grey, respectively. The preferred binding sites in each case are indicated by arrows. (b) Comparison of the predicted binding energies from an empirical scaling scheme and DFT calculations for methanol (red triangles), ethylene glycol (blue diamonds), glycerol (black circles), and erythritol (green crosses) dehydrogenation intermediates on Pt(111), adapted with permission from Ref. [16].[16] Copyright [2012] {Springer US}.

A general rule has been established to predict the preferred binding sites (i.e., top, bridge, 3-fold as indicated in Figure 3(a)) and molecular configuration without the consideration of solvent effect. Over Pt(111), each species is found to favor the configuration that satisfies the gas-phase valencies of the respective binding C and O atoms. For C and O, the respective valencies are 4 and 2, as in methane and water molecules. As illustrated in Figure 3(a), all $C_3H_7O_3$ species prefer the Pt top site. While glyceraldehyde and dihydroxyacetone bind at the bridge site to satisfy both

C and O in the ketone or the aldehyde functional group. In addition, the orientation and arrangement of the hydroxyl groups should also be considered because: (1) intramolecular hydrogen bonding among these hydroxyl groups stabilizes the overall structure; (2) additional stabilization can be gained from the molecular orientation that maximizes the interactions between hydroxyl groups and the metal substrate. When glycerol becomes significantly dehydrogenated, these rules can be broken occasionally due to molecular strain or highly delocalized bonding. Besides Pt, such rules are generally applicable to other transition metals such as Pd, Rh, Ni. However, over Au, Ag, and Cu, noticeable deviations have been observed in part due to very week binding of C=C, or C=O bonds on these metal surfaces.

The valency rule for adsorbed molecular species is not a new concept. Classical bond-order conservation formulations has been discussed by Shustorovich,[75,76] Kua and Goddard,[77] and Abild-Pedersen et al.[78] The central idea is that the adsorption patterns of surface-bound molecules on well-define surface lattices as mentioned above can be exploited to predict stable adsorption configurations and binding energies, instead of carrying out DFT calculations. For metals (e.g., Pt, Pd), the level of agreement is exceptionally high.

The scaling relationship, rooted in similar concepts, for glycerol and its intermediates have been developed previously on Pt(111) in a solvent free condition and is expressed by Equations (1) and (2).[15,16]

$$BE_{C_3H_xO_3^*} = \sum_i p_{Ci} v_{Ci} + \sum_i p_{Oi} v_{Oi} + \sum_{i,j} p_{CiOj} v_{Ci} v_{Oj} + \sum_{i,j} p_{CiCj} v_{Ci} v_{Cj} + BE_{C_3H_8O_3} \quad (1)$$

$$v_i = \frac{n_{max} - n_{bond}}{n_{max}}, \quad (2)$$

where v_{Ci} and v_{Oi} describe the degree of undersaturation of central C and O atoms in $C_3H_xO_3$, as represented by Equation (2), where n_{max} is 4 for C and 2 for O based on the gas-phase valence rule, and n_{bond} represents the total neighbors to which the central C/O atom is bonded (counting H, C, and O only). The last term ($BE_{C_3H_8O_3}$) in Equation (1) is the binding energy of gas phase glycerol on Pt(111). In Equation (1), p_{Ci}, p_{Oi}, p_{CiOj}, and p_{CiCj} are fitting parameters obtained from DFT calculations.[15] As illustrated in Figure 3(b), the scheme has been proven to predict binding energies of polyols (ethylene glycol, erythritol, and methanol all with C:O = 1:1 in these molecules) quite well, with an averaged error of 0.11 eV, using the same set of parameters derived only from glycerol intermediates on Pt(111). Due to the relevance of glycerol transformations in the aqueous phase, a keen interest is to explore whether or not such a scaling relationship can be adopted to predict energetic trends in adsorbed oxygenated hydrocarbons in the presence of water.

Recent efforts to understand interactions between liquid water and sugar alcohol adsorbates have been reported by Getman and co-workers in a series of combined periodic DFT and molecular dynamics simulations.[79,80] It has been shown that water molecules near adsorbates re-orient to form hydrogen bonds. In our *bottom-up* explicit-solvent model construction, two measures have been taken to simplify the model structures with account of solvent molecules (i.e., water) and intermolecular hydrogen bonding. First, the solvation contribution to adsorption energies can be broken down as water-metal, water-adsorbate, and water-water interactions. Second, only the first water overlayer is included in the model. The binding energy of $C_3H_xO_3^*(aq)$, where x = 0–8 in the presence of n explicit H_2O molecules, is denoted as $BE_{C_3H_xO_3^*(aq),DFT}$, and calculated from Equation (3).

$$BE_{C_3H_xO_3^*(aq),DFT} = E_{C_3H_xO_3^*(aq)} - E_* + \frac{8-x}{2}E_{H_2(g)} - E_{glycerol(g)} - nE_{H_2O(g)}, \quad (3)$$

In Equation (3), the total energy of adsorbate on Pt(111) is represented by $E_{C_3H_xO_3^*(aq)}$. Clean Pt(111) surface, gas phase H_2, glycerol, and H_2O is used as the zero potential energy reference, represented by E_*, $E_{H_2(g)}$, $E_{glycerol(g)}$, and $E_{H_2O(g)}$, respectively. This definition can be interpreted as a representation of the energetic tendency for $C_3H_xO_3$ to form covalent bond(s) upon adsorption, upon removal of $(8-x)$ hydrogen atoms in the form of gas phase H_2 molecules. In addition, the energy change also include the formation of water-water, water-adsorbate, and water-Pt(111) pair interactions, mostly in terms of hydrogen bonding.

For the scaling relationship, we assume that the first four terms on the right-hand side of Equation (1) remain the same as they account for valency-dependent (non-zero v_{Ci} and v_{Oi}) covalent bonding. In the case of glycerol, all v_{Ci} and v_{Oi} are zeroes. Then, the solvation effect can be collectively expressed by ξ, as in Equation (4).

$$\xi = \varepsilon_{ads-H_2O} + \varepsilon_{M-H_2O} + \varepsilon_{H_2O-H_2O}, \quad (4)$$

where contributions (associated with the solvent) from water-adsorbate, water-metal, and water-water interactions are represented by ε_{ads-H_2O}, ε_{M-H_2O}, and $\varepsilon_{H_2O-H_2O}$, respectively. The quantification of each term in Equation (4) and computational details are presented in the following sections.

The binding energy of glycerol in the aqueous phase, $BE_{C_3H_8O_3(aq)}$, can be written as Equation (5).

$$BE_{C_3H_8O_3(aq)} = \varepsilon_{gly-M} + \xi \quad (5)$$

where ε_{gly-M} is the binding energy of glycerol on metal (M). On Pt(111), this value (solvent free) is -0.46 eV.[15]

Coupled with the scaling scheme, the general form for binding energy of an arbitrary intermediate ($C_3H_xO_3$) in the aqueous phase becomes

$$BE_{C_3H_xO_{3(aq)}^*} = \sum_i p_{Ci} v_{Ci} + \sum_i p_{Oi} v_{Oi} + \sum_{i,j} p_{CiOj} v_{Ci} v_{Oj} + \sum_{i,j} p_{CiCj} v_{Ci} v_{Cj} + BE_{C_3H_8O_3(aq)}. \quad (6)$$

A comparison between Equations (1) and (6) suggest that the main difference in binding energies in respective solvent free and solvated environment stems from the binding energy of glycerol. Hence, it is anticipated from Equations (5) and (6) that, in an ideal situation where the impact of the solvent effect on an intermediate closely resemble to that of glycerol (i.e., ξ being a constant), $BE_{C_3H_xO_{3(aq)}^*}$ shall follow the original scaling trend dictated by Equation (1), except with a constant shift. In the following sections, periodic DFT calculations were carried out on glycerol, as well as a number of selected dehydrogenation intermediates to validate this hypothesis.

Periodic DFT calculations have been employed to obtain optimized structures. The results reported here were obtained using the Vienna *Ab initio* Simulation Package (VASP).[81,82] The computational parameters remain the same as in Ref. [15] in order to maintain consistency with scaling relationship development. The electronic one-particle wave function was expanded up to an energy cutoff of 380 eV. Convergence tests on the energy cutoff (up to 450 eV) using co-adsorbed glycerol and water molecule show that the binding energy change is within 10 meV. A Monkhorst-pack k-point mesh of 4 × 4 × 1 was used to sample the reciprocal first Brillouin zone.[83] The convergence criteria for self-consistent iteration and the ionic relaxation are 1×10^{-6}

eV and 0.02 eV/Å, respectively. The Methfessel-Paxton smearing at $k_B T = 0.2$ eV was used, and the total energies were then extrapolated to 0 K. Dipole correction were included in all calculations.

The close-packed planar platinum surface is modeled with the Pt(111) facet using a 3-layer $p(4 \times 4)$ supercell. The bottom two layers were fixed to the optimized platinum bulk lattice value at 3.98 Å. The top layer of Pt(111), adsorbate, and water molecules were allowed to relax.

The binding energies reported here are not corrected to account for van der Waals interactions. In polar solvents (e.g., water), electrostatic interactions typically dominate (over van der Waals interactions) in systems consisting of polar or ionic solutes.[84] Nevertheless, van der Waals interactions described at the DFT-D3 level have been shown to alter the adsorption structures of adsorbed alcohols such as ethanol even without the presence of solvent.[85-90] In order to fully integrate this non-covalent effect, it is necessary that the scaling relationship itself be further verified in future refinement.

INTERACTIONS BETWEEN WATER AND PT(111)

Compared to the covalent interactions between surface and adsorbate, water-metal interactions are relatively weak. Periodic DFT calculations reported in the literature show that the adsorption energies of a single water molecule on the (111) facet of transition metals vary between -0.1 – -0.4 eV in the order of Au < Ag < Cu < Ni < Pd < Pt < Ru < Rh.[91-94] The absolute value and exact order are sensitive to bulk lattice constant, size of unit cell and computational method. An isolated water molecule binds parallel to metal tops site via the lone pair electrons located on oxygen. Heras and Viscido[95] showed that, on Fe, Co, Ni, Pt, Cu, Au, water adsorptions lower the work function on all metals under the UHV condition. Filhol et al.[96] and

Schnur et al.,[60] further suggested that the change of work function is sensitive to the orientation of the water bilayer. Specifically, the H-up bilayer configuration is mainly responsible for the decrease of work function on Au, Ag, Pt, and Ru. On Ru, water dissociates, and the half-dissociated water layer plays the role in lowering work function.

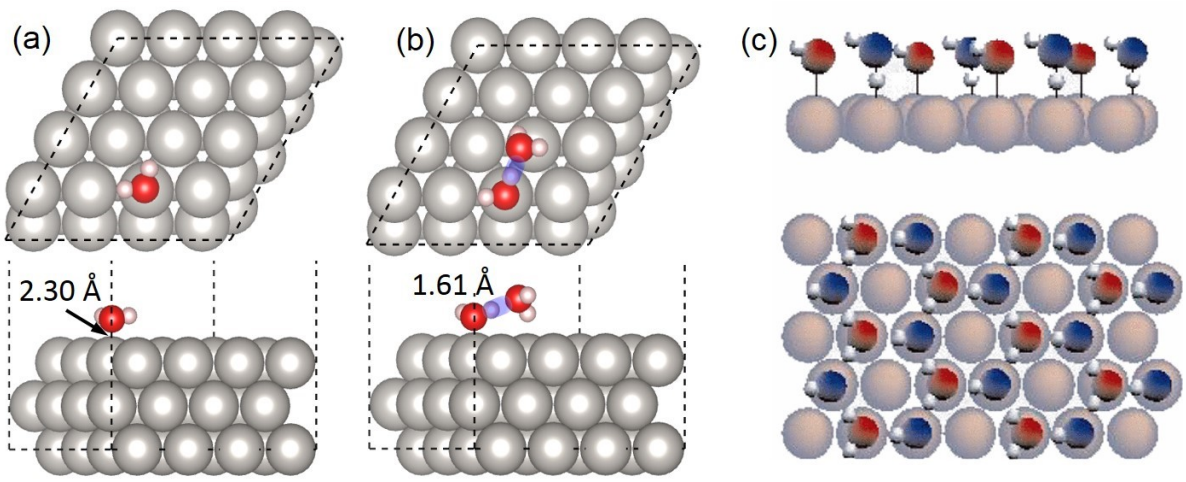

Figure 4. Adsorptions of (a) single H_2O, and (b) two adjacent H_2O molecules on Pt(111). The O–Pt bond distance (2.30 Å) in (a), and H–O bond distance (1.61 Å) in (b) are listed. The hydrogen bond between two H_2O molecules is indicated by the violet bar. Supercell boundaries are shown in black dashed lines. O, H, and Pt atoms are shown in red, pink and grey, respectively. (c) Illustration of the 'H-down' water bilayer configuration on Pt(111) adapted with permission from Ref. [54].[53] Copyright [2002] {American Physical Society].

Our calculation showed the binding energy of an isolated H_2O molecule on Pt(111) is -0.31 eV, with the distance between O and Pt being 2.30 Å, as indicated in Figure 4(a), and is in good agreement with prior report in the literature.[37] This value is also equivalent to the Pt-H_2O interaction energy. Hence, the value is assigned to ε_{Pt-H_2O}, as in Equation (7).

$$\varepsilon_{Pt-H_2O} = -0.31\ eV \tag{7}$$

To mimic the water-water interaction, a second water molecule is added to the first H_2O adsorbate, creating a water dimer. The optimized structure of the second water is positioned in a tilted H-down position as illustrated in Figure 4(b), resembling a sub-unit of the H-down water bilayer in Figure 4(c). A hydrogen bond, with a bond length of 1.61 Å highlighted in a violet bar in Figure 4(b), is formed between the two waters.

The overall binding energy of these co-adsorbed H_2O molecules is -0.91 eV, relative to water molecules in the gas phase. By excluding the contribution from the first H_2O molecule, i.e., ε_{Pt-H_2O} (-0.31 eV), and the interaction between Pt(111) and the second water and Pt(111) (i.e., -0.07 eV, obtained from a static calculation after the removal of the first H_2O), the net water-water interaction is -0.53 eV. The negative sign indicates that the interaction between this water dimer stabilizes the water dimer structure. This value is actually higher than the interaction between two water molecules (-0.24 eV) in the gas phase, suggesting that the substrate further enhances the clustering of co-adsorbed water molecules. Here, $\varepsilon_{H_2O-H_2O}$ assumes the value of -0.53 eV, as in Equation (8).

$$\varepsilon_{H_2O-H_2O} = -0.53\ eV \tag{8}$$

INTERACTIONS BETWEEN WATER AND ADSORBED GLYCEROL ON PT(111)

In the absence of water, we have shown that glycerol binds at the top site via the oxygen atom in one of the terminal hydroxyl groups on Pt(111).[15] It has been confirmed that the nature of such interaction originates from oxygen's lone pair electrons. For glycerol, an intramolecular hydrogen bond exists between the two terminal hydroxyl groups, as indicated by the green bars in Figure 5(a-f), while the middle hydroxyl group tilts away from the surface in the opposite direction.

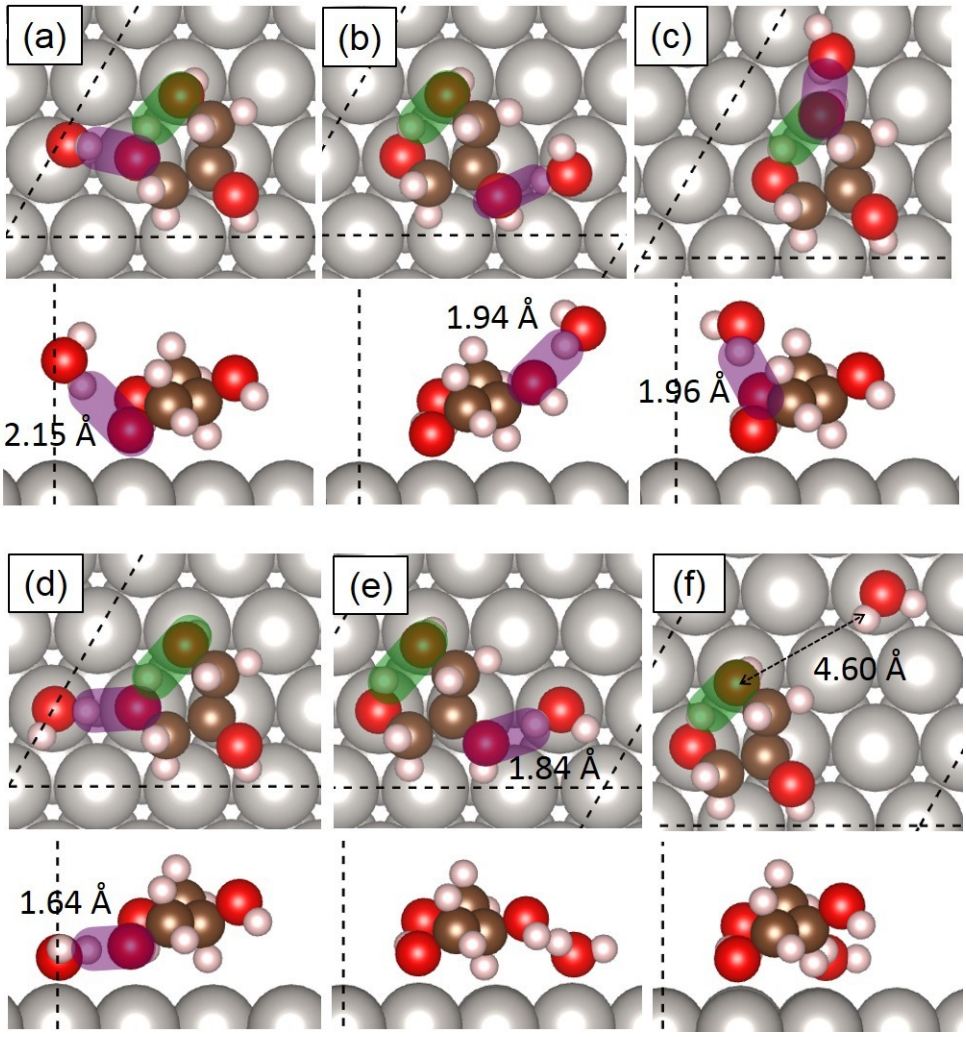

Figure 5. Top and side views of glycerol and water co-adsorbed on Pt(111) in various scenarios (a-f). C, O, H, and Pt atoms are shown in brown, red, pink and grey, respectively. The intramolecular hydrogen bond is highlighted with green bars; intermolecular hydrogen bonds between water and glycerol are highlighted in purple, with bond lengths labeled. Supercell boundaries are shown in black dashed lines.

The structure of adsorbed glycerol on Pt(111) without solvent is used as the starting point. Water (i.e., the first H_2O added) is used to probe the potential energy surrounding the adsorbed glycerol. In configurations Figure 5(a-c), water is deliberately separated from Pt(111) to

minimize its interactions with the substrate. A close distance is maintained so that water is still capable of interacting with one of the hydroxyl groups (highlighted by purple bars). The intermolecular hydrogen bond lengths in configurations (a-c) are 2.15, 1.94, and 1.96 Å, respectively. In configurations (d) and (e), water molecules are placed directly above Pt(111) so that water-metal interactions can be enabled. In both cases, water still prefers to bind on the Pt top site while maintaining the intermolecular hydrogen bonding with glycerol, at a distance of 1.64 Å and 1.84 Å, respectively. The intramolecular hydrogen bonding shown in green bars, in both cases, is preserved. In Figure 5(f), the water molecule co-adsorbed with glycerol is deliberately separated at a distance of 4.60 Å (as indicated by the double-headed arrow), to minimize a direct adsorbate-water interaction.

Binding energies ($BE_{C_3H_8O_3^*(aq),DFT}$) of obtained from configurations (a-f) are summarized in Table 1, determined from Equation (3) at n = 1 and x = 8. The most energetically favorable configuration is (d), in which the overall binding energy is -1.07 eV. Configuration (a), on the other hand, is the least energetically favored. This result signifies the importance of water-metal interactions at the interface, and showed that the adsorbate does not exclude co-adsorbed water in its proximity. The binding energy of configuration (f) is 0.23 eV higher than configuration (d). This difference can be considered as the interaction energy between glycerol and water, assuming that the values ε_{Pt-H_2O}, are similar. Hence, ε_{gly-H_2O} for glycerol-water interaction, as in Equation (9), can be approximate as -0.23 eV. Again, the minus sign indicates that this interaction stabilizes the co-adsorbed structure.

$$\varepsilon_{gly-H_2O} = -0.23\ eV \tag{9}$$

Table 1. Binding energies of co-adsorbed of glycerol and single H_2O molecule ($BE_{C_3H_8O_3^*(aq),DFT}$ in eV) on Pt(111).

Configuration	(a)	(b)	(c)	(d)	(e)	(f)
$BE_{C_3H_8O_3^*(aq),DFT}$	-0.66	-0.78	-0.79	-1.07	-0.99	-0.84

To include water-water interactions, the number of water molecules (n) is increased incrementally (up to 12). The most stable structure for each n value is illustrated in Figure 6(a-g). At $n = 2$ in Figure 6(b), the second water molecule (highlighted in a yellow circle) prefers the location that enables the formation of an intermolecular hydrogen bond (highlighted in blue) with the first water molecule. In addition, the second water molecule is in the H-down position, resembling the structure identified in Figure 4(b). This way, all co-adsorbed species are in their preferred configuration. Thus, the system consists of two intermolecular hydrogen bonds (i.e., water-water and water-glycerol), and one intramolecular hydrogen bond from the structure of adsorbed glycerol.

At $n = 3$ in Figure 6(c), the third water (highlighted in a yellow circle) is added to extend the water chain, resulting one additional intermolecular hydrogen bond (blue bar). Moreover, it can be seen that the extended structure enables this water to interact with the glycerol's own periodic image (through the middle hydroxyl group) in the neighboring supercell. Hence, a continuous (1-D) network centered on the adsorbate that is inter-connected its periodic images via water molecules, is established.

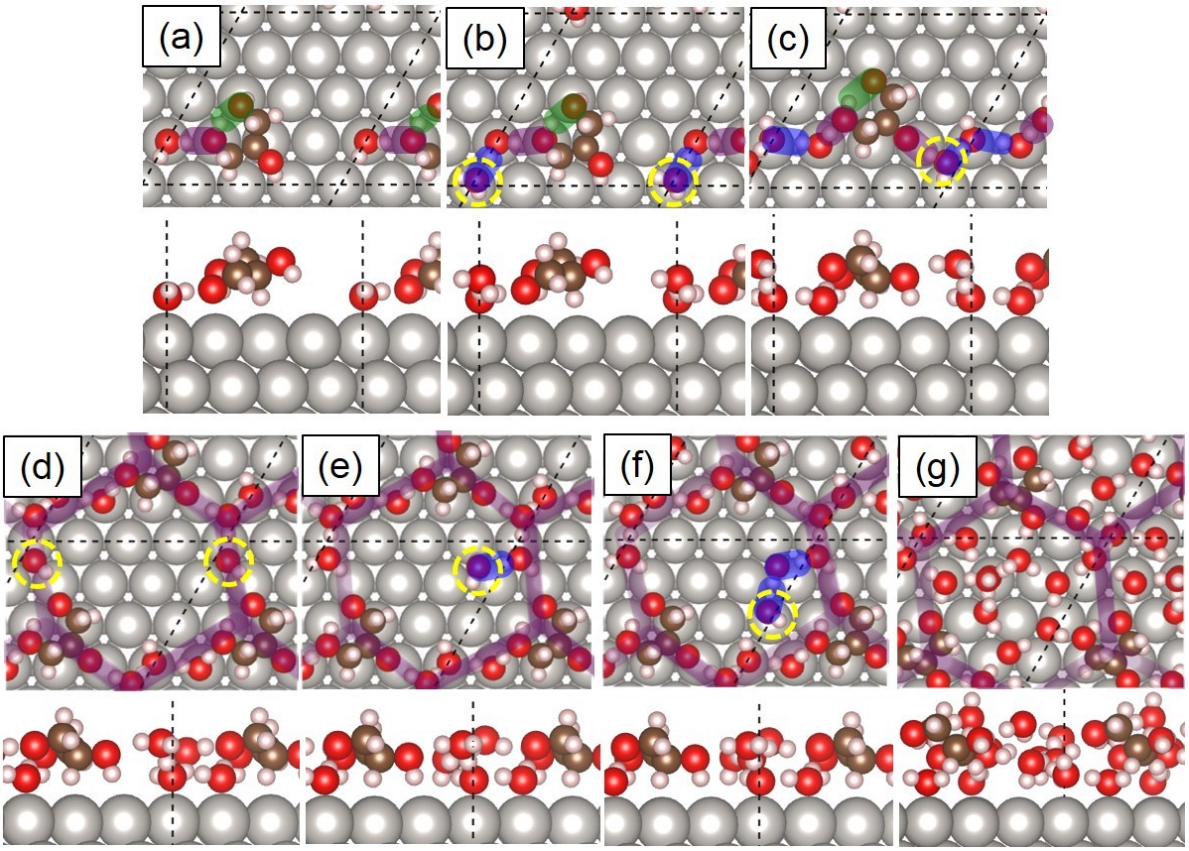

Figure 6. Co-adsorption of glycerol on Pt(111)with (a) 1 H_2O, (b) 2 H_2O, (c) 3 H_2O, (d) 4 H_2O, (e) 5 H_2O, (f) 6 H_2O, and (g) 12 H_2O molecules. C, O, H, and Pt atoms are in brown, red, pink and grey, respectively. Green, purple, and blue bars in (a-c) indicate the intramolecuar hydrogen bond, glycerol-water, and water-water hydrogen bonding, respectively. Supercell boundaries are shown in black dashed lines.

At $n = 4$ in Figure 6(d), the fourth water molecule (highlighted in the dashed yellow circle) continues to contribute to the growth of the established water network by interacting with the other terminal hydroxyl group facilitated by the periodicity of the supercell. At this stage, a close-loop structure, in an approximate hexagonal shape (highlighted in purple to guide visualization), is formed. All the hydroxyl groups available in glycerol are now able to coordinate with one water molecule.

The additions of the fifth and sixth water molecules are depicted in Figure 6(e-f), respectively. Since there is no free hydroxyl group in glycerol to accept additional water molecules, the fifth and sixth water can only be added to the existing water network. All intermolecular hydrogen bonds are indicated with blue bars. In Figure 6(f), with six water molecules, a secondary five-member ring is formed.

When twelve water molecules are added, the remaining open space of Pt(111) is being occupied, resulting a surface now fully covered with glycerol and a water overlayer, as illustrated in Figure 6(g), consisting of five- or six-membered water rings. Such water formation has been reported by Nie and coworkers,[56] who confirmed the existence of a mixture of five-, six-, and seven-membered rings with the $\sqrt{37}$ and $\sqrt{39}$ periodic wetting arrangement on Pt(111) from scanning tunneling topography measurements and DFT calculations.

It can be seen that the growth initiates from the adsorbed glycerol, and then expands from its anchoring hydroxyl groups. As the number of water molecules increases, the water structure evolves from a linear structure to a hexagonal network through water-water interactions. The first-layer water molecules still maintain a close contact with Pt(111). Intermolecular hydrogen bonding between as many hydroxyl groups and water is satisfied.

The binding energies of adsorbed glycerol ($BE_{C_3H_8O_3^*(aq),DFT}$) calculated from Equation (3) with n H_2O molecules, as illustrated in Figure 6(a-g), are tabulated in Table 2. The values of $BE_{C_3H_8O_3^*(aq),DFT}$ incrementally decrease by approximately $0.5-0.6$ eV with each additional H_2O added, coinciding with the value of $\varepsilon_{H_2O-H_2O}$. The differential binding energies per H_2O are also plotted in Figure 7 (black stars). The upward trend indicates that the energetic gain diminishes with each additional water as fewer favorable locations are available to form hydrogen bonding. Additional water molecules is expected to form the second water overlayer.

Table 2. Calculated $BE_{C_3H_8O_3^*(aq),DFT}$ (in eV) on Pt(111) at different n values.

n	1	2	3	4	5	6	12
$BE_{C_3H_8O_3^*(aq),DFT}$	-1.07	-1.65	-2.23	-2.90	-3.32	-3.82	-7.62

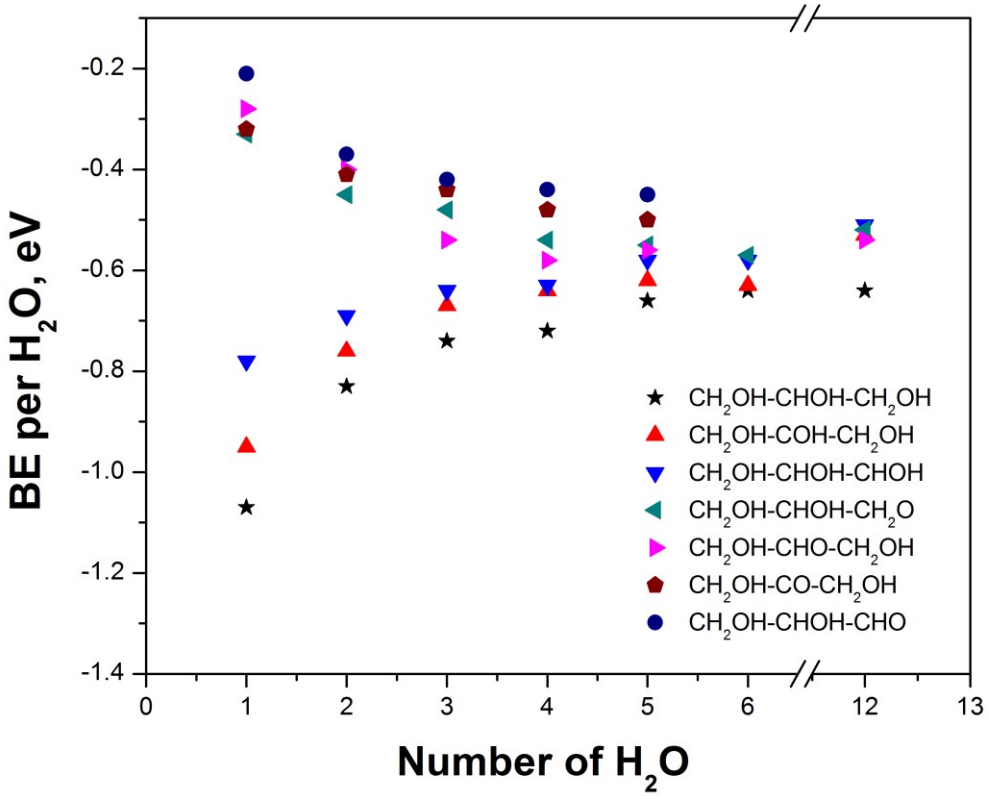

Figure 7. DFT-calculated $BE_{C_3H_xO_3^*(aq).DFT}$ (x = 0-8) per H_2O at different numbers of H_2O on Pt(111).

INTERMEDIATES ON PT(111) AND SCALING RELATIONSHIP

Adsorptions of glycerol dehydrogenation intermediates on Pt(111)

In this section, we aim to validate the hypothesis brought up previously to show if the predicted binding energies of other glycerol-based dehydrogenation intermediates will still

follow the scaling relationship in the aqueous phase (possibly with a constant shift due to ξ). Glycerol dehydrogenation via C-H or O-H bond scission is a main route for the production of hydrogen, as well as numerous value-added chemicals such as dihydroxyacetone, lactic acid, 1,2-propanediol, alcohols and alkanes.[97,98] In this work, four mono-dehydrogenated ($C_3H_7O_3$) and up to ten di-dehydrogenated intermediates ($C_3H_6O_3$) were chosen. Among the $C_3H_6O_3$ species, dihydroxyacetone (CH_2OH-CO-CH_2OH) and glyceraldehyde (CH_2OH-$CHOH$-CHO) are two stable and also marketable dehydrogenation products, which can be produced selectively from electrooxidation.[4]

Optimized configurations for each selected $C_3H_xO_3$ intermediates (x = 6, 7) were obtained on Pt(111), using structures from vapor phase calculations for relaxation. Water molecules were introduced in a similar manner, largely informed by the patterns observed in Figure 6. For the majority of intermediates, we found that five water molecules are needed to form closed network structures on the surface. The most stable configurations for $C_3H_7O_3$ and $C_3H_8O_3$ co-adsorbed with five water molecules are illustrated in Figures (8) and (9), respectively.

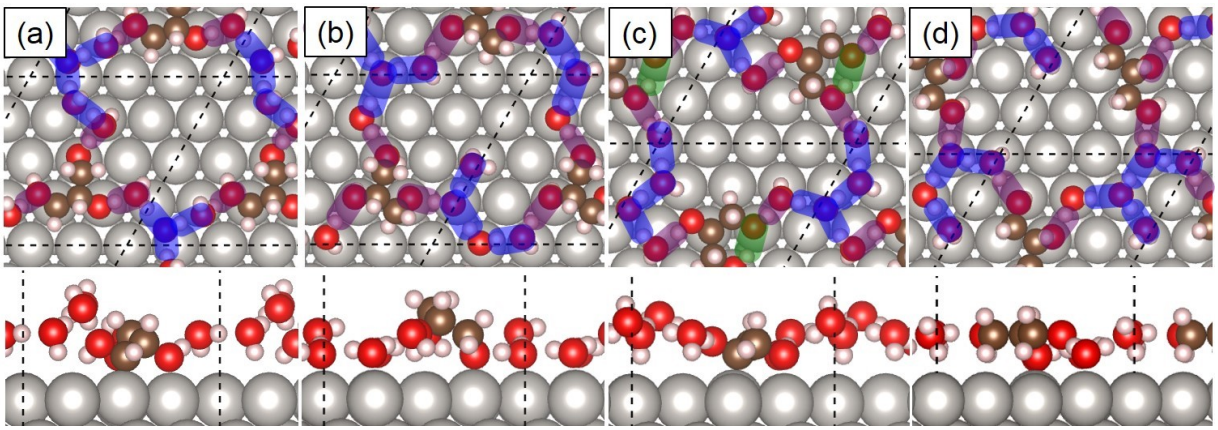

Figure 8. Top and side views of the four $C_3H_7O_3$ intermediates, (a) CH_2OH-$CHOH$-$CHOH$, (b) CH_2OH-$CHOH$-CH_2O, (c) CH_2OH-COH-CH_2OH, and (d) CH_2OH-CHO-CH_2OH, with five water molecules on Pt(111) in their most stable configurations. C, O, H, and Pt atoms are

shown in brown, red, pink and grey, respectively. Green, purple, and blue bars highlight intramolecuar hydrogen bond, adsorbate-water, and water-water interaction, respectively. Supercell boundaries are shown in black dashed lines.

The binding sites for all four $C_3H_7O_3$ intermediates remain unchanged at the top site of Pt(111), as illustrated in Figure 8(a-d). Again, the intramolecuar hydrogen bond, adsorbate-water, and water-water interactions are distinguished by the green, purple, and blue bars. Through co-adsorbed water molecules, adsorbates forms familiar continuous networks with their periodic images across the unit cell boundaries. Despite the ideal situation facilitated by such a specific periodic boundary condition, we believe the predicted molecular structures presented in Figures 8 and 9 still provide the insights into the direct interactions among adsorbate, solvent, and substrate at the interface that cannot be probed straightforwardly otherwise. As highlighted in purple in Figure 8, all three hydroxyl groups have to be involved in establishing connections linked by water molecules through hydrogen bonding. Similar observations were made for many of the $C_3H_6O_3$ intermediates illustrated in Figure 9 as well.

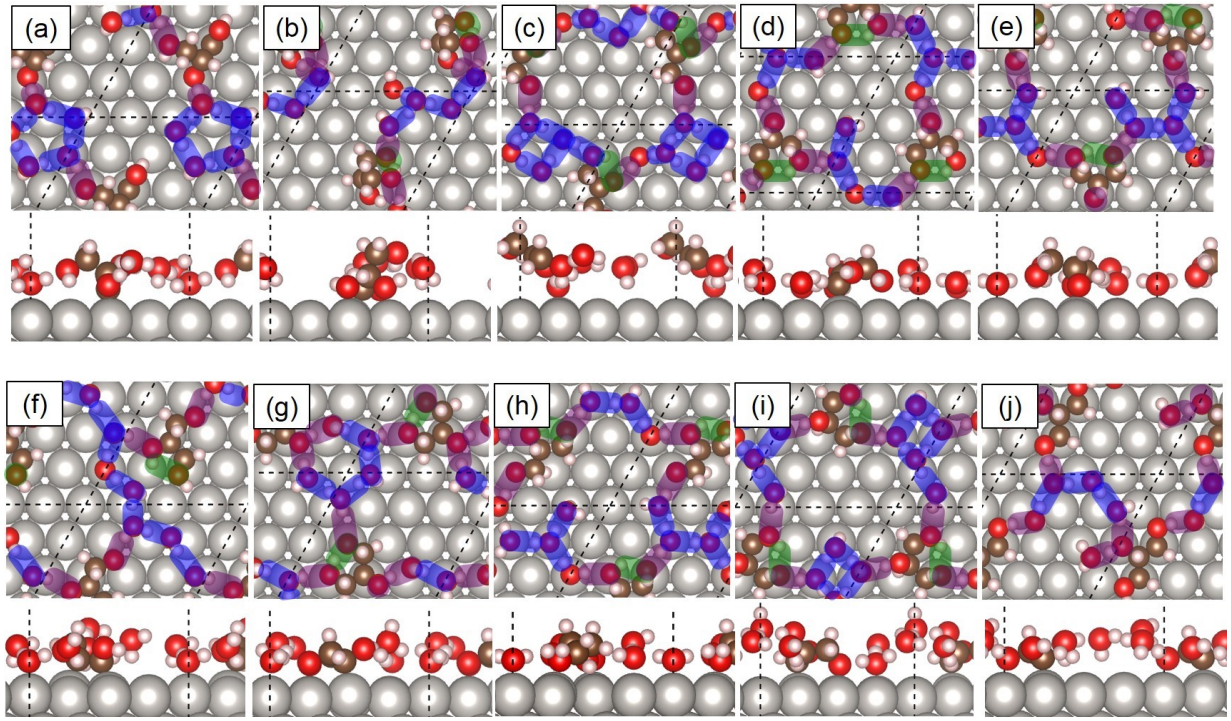

Figure 9. Top and side views of ten selected $C_3H_6O_3$, co-adsorbed with five water molecules on Pt(111) in their most stable configurations. (a) CH_2OH-CHOH-COH, (b) CH_2OH-CHOH-CHO, (c) CH_2OH-CO-CH_2OH, (d) CH_2OH-CHO-CHOH, (e) CH_2OH-CHO-CH_2O, (f) CH_2OH-COH-CHOH, (g) CH_2OH-COH-CH_2O, (h) CH_2O-CHOH-CH_2O, (i) CHOH-CHOH-CH_2O, and (j) CHOH-CHOH-CHOH. C, O, H, and Pt are in brown, red, pink and grey, respectively. Green, purple, and blue bars highlight intramolecuar hydrogen bond, adsorbate-water, and water-water interaction, respectively. Supercell boundaries are shown in black dashed lines.

The binding energies, calculated from Equation (3), for the four $C_3H_7O_3$, dihydroxyacetone, and glyceraldehyde with $n = 0, 1, 5$ co-adsorbed water molecules, are tabulated in Table 3. At $n = 0$ (solvent free), it is known that the intermediates from C-H bond scission are more stable than those from O-H bond scission (with the same stoichiometry) on Pt(111).[15] At $n = 1$, binding for all intermediates becomes stronger (i.e., more negative) due to the attractive interactions (ε_{gly-H_2O} and ε_{Pt-H_2O}) provided by the water on a rather open surface. At $n = 5$, $BE_{C_3H_xO_3^*(aq),DFT}$ become less negative for the two intermediates that bind with C, but are still

lower (more negative) than those when no water was added. The molecular perspective obtained indicates that the energetic difference during glycerol dehydrogenation could be diminished due to the solvation effect.

The calculated $BE_{C_3H_xO_3^*(aq),DFT}$ per H_2O for these dehydrogenation intermediates are also shown in Figure 7. It becomes clear that, with the increase of water molecules, binding energies of glycerol and intermediates that bind with C become less negative; but an opposite trend is observed for intermediates that bind with unsaturated O. In the high water coverage limit considered, binding energies for selected intermediates converge to within 0.2 eV.

Table 3. Comparisons for $BE_{C_3H_xO_3^*(aq),DFT}$ (x = 6, 7, in eV) at $n = 0, 1, 5$ using Equation (3).

Species	$BE_{C_3H_xO_3^*(aq),DFT}$, $n = 0$	$BE_{C_3H_xO_3^*(aq),DFT}$, $n = 1$	$BE_{C_3H_xO_3^*(aq),DFT}$, $n = 5$
CH_2OH-COH-CH_2OH	-0.27	-0.95	-0.62
CH_2OH-$CHOH$-$CHOH$	-0.19	-0.78	-0.58
CH_2OH-$CHOH$-CH_2O	0.41	-0.33	-0.55
CH_2OH-CHO-CH_2OH	0.45	-0.28	-0.57
CH_2OH-CO-CH_2OH	0.48	-0.32	-0.50
CH_2OH-$CHOH$-CHO	0.53	-0.21	-0.45

Scaling Relationship for Solvated Systems

It is mentioned that a scaling relationship based on valences of unsaturated C and/or O exists in a solvent-free environment.[15] Here, we set out to re-examine this formulation, i.e., Equations (2) and (6), by incorporating water-adsorbate, water-metal, and water-water interactions. $BE_{C_3H_xO_3^*(aq),DFT}$, denoted as BE (DFT) in Figure 10, are evaluated based on Equation (3), at $n = 5$.

Because configuration of each adsorbate does not vary significantly, the covalent interaction in $BE_{C_3H_xO_3^*(aq)}$ between adsorbate and metal can be assumed intact. The ξ term in Equation (4) is composed of contributions from four hydrogen bonding between water molecules ($4\varepsilon_{H_2O-H_2O}$), two hydrogen bonding between glycerol and water ($2\varepsilon_{gly-H_2O}$,), and water-Pt(111) interactions from two water molecules ($2\varepsilon_{Pt-H_2O}$). By simple summation, ξ is calculated as -3.20 eV. Combined with ε_{gly-M}, $BE_{C_3H_8O_3^*(aq)}$ is -3.66 eV from Equation (5).

The comparison between BE (DFT) and $BE_{C_3H_xO_{3(aq)}^*}$ from Equation (6), denoted as BE (scaling), are shown in Figure 10(a). The standard errors associated with the scaling for $C_3H_7O_3$ and $C_3H_6O_3$ are 0.20 eV and 0.17 eV, respectively. It can be seen that all BE (DFT) have shifted downward by 0.34 eV from the parity line ($y = x$). The shift originates from the difference between $BE_{C_3H_8O_3^*(aq),DFT}$ (-3.32 eV at $n = 5$) and the binding energy of glycerol obtained from Equation (5) (-3.66 eV). In fact, the shift can be eliminated when $BE_{C_3H_8O_3^*(aq),DFT}$, is used in Equation (6) to generate the scaling relationship, as shown in Figure 10(b).

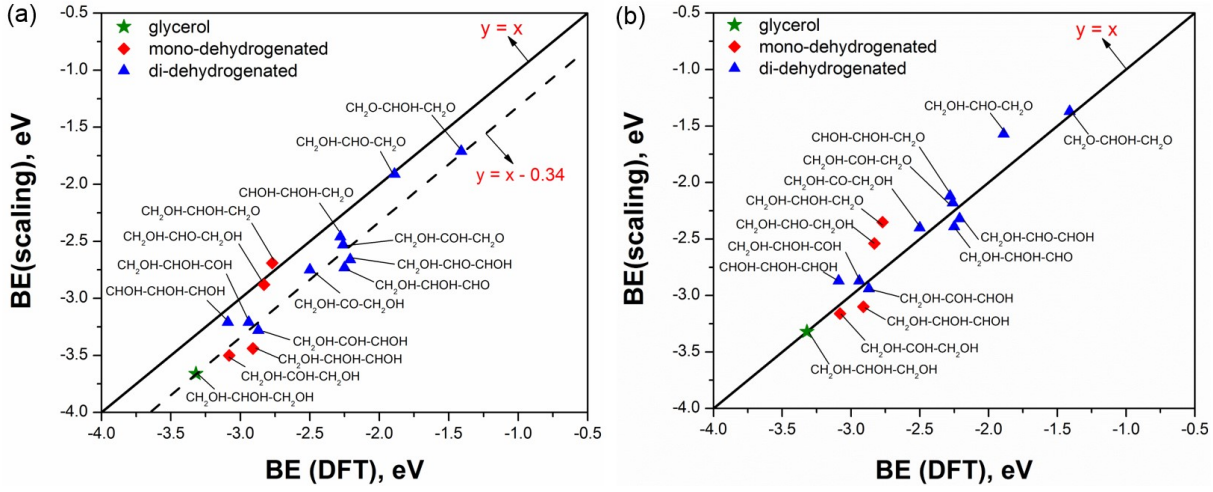

Figure 10. Relationship between DFT calculations from Equation (3) and scaling based on

Equations (2, 4-6), for glycerol (green star), $C_3H_7O_3$ (red diamonds) and $C_3H_6O_3$ (blue triangles) with five H_2O molecules on Pt(111).

The observed constant energy shift invokes a common notion in the computational community that solvent often indiscriminately affects the binding energies of structurally similar adsorbates. The accompanying energetic analysis confirms this long-standing belief for adsorbed glycerol and its intermediates. It should also be pointed out that, despite the fact that a general agreement, the binding of CH_2OH-$CHOH$-CH_2O, CH_2OH-CHO-CH_2OH, and CH_2OH-CHO-CH_2O, as in Figure 8(b), 8(d), and 9(e) show noticeable deviation from the scaling relationship and their values are underestimated. The underlying cause to such deviation can be attributed to significant variation in adsorption configuration of these adsorbates from glycerol. This can interpreted that certain adsorbates on solid surface are likely undergo structure transformation upon solvation. In order to reconcile with the predictions of the scaling relationship, new configurations for these intermediates must be tested.

CONCLUSIONS AND OUTLOOK

Driven by the ever growing computational toolsets and computing power, the modeling capacity has achieved remarkable breakthrough in the last few decades. High-level molecular modeling of sophisticated systems, so that direct comparisons with realistic environment, has become routine research tasks. In this work, we tackled an important aspect of catalytic glycerol processing in the aqueous phase environment by investigating the adsorption patterns of glycerol and its dehydrogenation intermediates at the metal-liquid interface. By using the explicit solvation approach, extensive network structures established by adsorbates and co-adsorbed

water molecules were elucidated through periodic DFT calculations. As a result, specific metal-water, water-water and adsorbate-water interactions on Pt(111) are described using simple pairwise interaction energy concepts. We found that although interaction of water with polar adsorbates, metal, and other water molecules are always attractive in nature, the net impact on adsorption energies vary. Compared to the solvent free systems, stronger binding intermediates generally experience a 'weakening' effect, while, on the other hand, weaker binding intermediates benefits from the existence of water to bind on Pt(111). Here, the scaling relationship has been re-evaluated by including various solvent-related molecular interactions. It is believed that this strategy shall continue to play an important role in minimizing unnecessary computational costs while detailed molecular information is still required for structural and mechanistic analyses.

Despite the promising trend presented in this article, it should be noted that molecular structures at metal-liquid interface are delicate and dynamic. Moving forward, several technical issues need to be addressed so that the predictive power of the solvation and computational capability and efficiency can be further improved.

First, the water structures can vary greatly from metal to metal. As pointe out by Carrasco and Michaelides,[55] the wetting layer does not always show as in the bilayer form, but as OH-H_2O overlayer. The partially dissociated water can certainly disrupt the adsorption patterns observed in this work. More importantly, some of these systems can be quite relevant in the context of glycerol reforming. Water structures can also be sensitive to surface conditions, for instance, hydrogen coverage. Schnur and Groß[60] showed that distance between water overlayer and H-covered surface increases. Beyond hydrogen and some very simple adsorbate species, understanding of water structures at metal surfaces is still scare. Such information is potentially

critical, since better descriptions of water structure, coupled with thorough consideration of adsorbate configurations on metal surfaces, is essential to improve the accuracy and reliability.

The second question is: can different techniques be smoothly integrated to overcome the deficiency of standard periodic DFT calculations? If a classical potential is available for the metal-water interface, molecular dynamics simulations, conducted with larger simulation boxes, could offer desirable descriptions of key thermodynamic properties (e.g. enthalpy and entropy) of the solution phase; and also lower interference by unwanted size effects. Work by Getman et al.[79] has shown promise to expand the modeling capacity for the bulk solvation component of the system. Alternatively, *ab initio* molecular dynamics (AIMD) provides the desirable feature to obtain the dynamic information of aqueous phase water at elevated temperatures without need for the availability of water-metal force field potentials.[60,71,99-104] As discussed, implicit solvation models are powerful modeling techniques. Recent works focusing on hybrid implicit model containing a few explicit solvent molecules shall be an interesting trend in the near future.

Thirdly, because of the significance of aqueous phase chemistries in various electrochemical systems related to renewable chemicals and fuels productions,[105,106] adapting standard modeling practices to tackle charged system and charge transfers in electrochemical reaction remains a booming research direction. The linear free energy relationship (LFER), represented by the so-called computational hydrogen electrode (CHE) is a zeroth-order treatment of reactions involving charge transfer, and has been most widely applied in modeling. On the other hand, it is also shown that the surface charge method by Filhol and Neurock,[37] developed in parallel works, suits adsorbates with large dipole moments better. For electrified metal-liquid interfaces, Rossmeisl and coworkers[107] designed a simple extrapolation strategy to remove the finite size effect, which can be a common issue in periodic DFT calculations, by performing a series of

calculations using different supercell sizes. On a different front, methods to describe reaction kinetics of electrochemical systems have been devised recently. For instance, using the same strategy developed by Rossmeisl et al.,[107] Skulason et al.[70] obtained the energy barriers for the elementary Heyrovsky mechanism using a water bilayer model. Furthermore, the kinetics of CO_2 electroreduction elementary steps was studied by Nie and Janik[34,68], where the potential dependent energy barriers can be determined using transition states from non-electrochemical systems then extrapolated systems at specified electrochemical potentials.

AUTHOR INFORMATION

Corresponding Author

*B. Liu, E-mail: binliu@ksu.edu

ORCID

Nannan Shan: 0000-0002-7700-6246

Bin Liu: 0000-0001-7890-7612

Notes

The authors declare no competing financial interest.

ACKNOWLEDGMENTS

N.S., and B.L. thank the Start-up fund provided by Kansas State University. N.S. would also like to thank the summer support from the Erickson Fellowship. The authors are grateful for the supercomputing service provided by K-State Beocat Research Cluster funded in part by NSF grants CHE-1726332, CNS-1006860, EPS-1006860, and EPS-0919443; Center for Nanoscale Materials (CNM) at Argonne National Laboratory supported by the Office of Science of the US

Department of Energy under the contract No. DE-AC02-06CH11357; and the National Energy Research Scientific Computing Center (NERSC) under the contract No. DE-AC02-05CH11231.

REFERENCES

(1) Garcia, R.; Besson, M.; Gallezot, P., Chemoselective catalytic-oxidation of glycerol with air on platinum metals, *Applied Catalysis a-General,* **1995**, *127*, 165-176.
(2) Chheda, J. N.; Huber, G. W.; Dumesic, J. A., Liquid-phase catalytic processing of biomass-derived oxygenated hydrocarbons to fuels and chemicals, *Angewandte Chemie-International Edition,* **2007**, *46*, 7164-7183.
(3) Zhou, C.-H.; Beltramini, J. N.; Fan, Y.-X.; Lu, G. Q., Chemoselective catalytic conversion of glycerol as a biorenewable source to valuable commodity chemicals, *Chemical Society Reviews,* **2008**, *37*, 527-549.
(4) Kwon, Y.; Schouten, K. J. P.; Koper, M. T. M., Mechanism of the catalytic oxidation of glycerol on polycrystalline gold and platinum electrodes, *ChemCatChem,* **2011**, *3*, 1176-1185.
(5) Simoes, M.; Baranton, S.; Coutanceau, C., Electrochemical valorisation of glycerol, *Chemsuschem,* **2012**, *5*, 2106-2124.
(6) Nilges, P.; Schröder, U., Electrochemistry for Biofuel Generation: Production of Furans by Electrocatalytic Hydrogenation of Furfurals, *Energy & Environmental Science,* **2013**, *6*, 2925-2931.
(7) Parpot, P.; Bettencourt, A. P.; Chamoulaud, G.; Kokoh, K. B.; Beigsir, E. M., Electrochemical investigations of the oxidation-reduction of furfural in aqueous medium - Application to electrosynthesis, *Electrochimica Acta,* **2004**, *49*, 397-403.
(8) Green, S. K.; Lee, J.; Kim, H. J.; Tompsett, G. A.; Kim, W. B.; Huber, G. W., The Electrocatalytic Hydrogenation of Furanic Compounds in a Continuous Electrocatalytic Membrane Reactor, *Green Chemistry,* **2013**, *15*, 1869-1879.
(9) Liu, B.; Gao, F., Navigating Glycerol Conversion Roadmap and Heterogeneous Catalyst Selection Aided by Density Functional Theory: A Review, *Catalysts,* **2018**, *8*.
(10) Pagliaro, M.; Ciriminna, R.; Kimura, H.; Rossi, M.; Della Pina, C., From glycerol to value-added products, *Angewandte Chemie-International Edition,* **2007**, *46*, 4434-4440.
(11) Quispe, C. A. G.; Coronado, C. J. R.; Carvalho, J. A., Glycerol: production, consumption, prices, characterization and new trends in combustion, *Renewable & Sustainable Energy Reviews,* **2013**, *27*, 475-493.
(12) Ciriminna, R.; Della Pina, C.; Rossi, M.; Pagliaro, M., Understanding the glycerol market, *European Journal of Lipid Science and Technology,* **2014**, *116*, 1432-1439.
(13) Cortright, R. D.; Davda, R. R.; Dumesic, J. A., Hydrogen from catalytic reforming of biomass-derived hydrocarbons in liquid water, *Nature,* **2002**, *418*, 964.
(14) Luo, N.; Fu, X.; Cao, F.; Xiao, T.; Edwards, P. P., Glycerol aqueous phase reforming for hydrogen generation over Pt catalyst – Effect of catalyst composition and reaction conditions, *Fuel,* **2008**, *87*, 3483-3489.

(15) Liu, B.; Greeley, J., Decomposition Pathways of Glycerol via C–H, O–H, and C–C Bond Scission on Pt(111): A Density Functional Theory Study, *The Journal of Physical Chemistry C,* **2011**, *115*, 19702-19709.
(16) Liu, B.; Greeley, J., Density Functional Theory Study of Selectivity Considerations for C–C Versus C–O Bond Scission in Glycerol Decomposition on Pt(111), *Topics in Catalysis,* **2012**, *55*, 280-289.
(17) Auneau, F.; Michel, C.; Delbecq, F.; Pinel, C.; Sautet, P., Unravelling the Mechanism of Glycerol Hydrogenolysis over Rhodium Catalyst through Combined Experimental–Theoretical Investigations, *Chemistry – A European Journal,* **2011**, *17*, 14288-14299.
(18) Maris, E. P.; Davis, R. J., Hydrogenolysis of glycerol over carbon-supported Ru and Pt catalysts, *Journal of Catalysis,* **2007**, *249*, 328-337.
(19) Iriondo, A.; Barrio, V. L.; Cambra, J. F.; Arias, P. L.; Güemez, M. B.; Navarro, R. M.; Sánchez-Sánchez, M. C.; Fierro, J. L. G., Hydrogen Production from Glycerol Over Nickel Catalysts Supported on Al2O3 Modified by Mg, Zr, Ce or La, *Topics in Catalysis,* **2008**, *49*, 46.
(20) Iriondo, A.; Cambra, J. F.; Barrio, V. L.; Guemez, M. B.; Arias, P. L.; Sanchez-Sanchez, M. C.; Navarro, R. M.; Fierro, J. L. G., Glycerol liquid phase conversion over monometallic and bimetallic catalysts: Effect of metal, support type and reaction temperatures, *Applied Catalysis B: Environmental,* **2011**, *106*, 83-93.
(21) Dietrich, P. J.; Lobo-Lapidus, R. J.; Wu, T.; Sumer, A.; Akatay, M. C.; Fingland, B. R.; Guo, N.; Dumesic, J. A.; Marshall, C. L.; Stach, E.; Jellinek, J.; Delgass, W. N.; Ribeiro, F. H.; Miller, J. T., Aqueous Phase Glycerol Reforming by PtMo Bimetallic Nano-Particle Catalyst: Product Selectivity and Structural Characterization, *Topics in Catalysis,* **2012**, *55*, 53-69.
(22) Dietrich, P. J.; Wu, T.; Sumer, A.; Dumesic, J. A.; Jellinek, J.; Delgass, W. N.; Ribeiro, F. H.; Miller, J. T., Aqueous Phase Glycerol Reforming with Pt and PtMo Bimetallic Nanoparticle Catalysts: The Role of the Mo Promoter, *Topics in Catalysis,* **2013**, *56*, 1814-1828.
(23) King, D. L.; Zhang, L.; Xia, G.; Karim, A. M.; Heldebrant, D. J.; Wang, X.; Peterson, T.; Wang, Y., Aqueous phase reforming of glycerol for hydrogen production over Pt–Re supported on carbon, *Applied Catalysis B: Environmental,* **2010**, *99*, 206-213.
(24) Liu, B.; Zhou, M.; Chan, M. K. Y.; Greeley, J. P., Understanding polyol decomposition on bimetallic Pt-Mo catalysts - A DFT study of glycerol, *ACS Catalysis,* **2015**, *5*, 4942-4950.
(25) Liu, B.; Greeley, J., A density functional theory analysis of trends in glycerol decomposition on close-packed transition metal surfaces, *Physical Chemistry Chemical Physics,* **2013**, *15*, 6475-6485.
(26) Chen, Y.; Salciccioli, M.; Vlachos, D. G., An efficient reaction pathway search method applied to the decomposition of glycerol on platinum, *The Journal of Physical Chemistry C,* **2011**, *115*, 18707-18720.
(27) Salciccioli, M.; Chen, Y.; Vlachos, D. G., Density Functional Theory-Derived Group Additivity and Linear Scaling Methods for Prediction of Oxygenate Stability on Metal Catalysts: Adsorption of Open-Ring Alcohol and Polyol Dehydrogenation Intermediates on Pt-Based Metals, *The Journal of Physical Chemistry C,* **2010**, *114*, 20155-20166.
(28) Coll, D.; Delbecq, F.; Aray, Y.; Sautet, P., Stability of intermediates in the glycerol hydrogenolysis on transition metal catalysts from first principles, *Physical Chemistry Chemical Physics,* **2011**, *13*, 1448-1456.
(29) García-Muelas, R.; López, N., Collective Descriptors for the Adsorption of Sugar Alcohols on Pt and Pd(111), *The Journal of Physical Chemistry C,* **2014**, *118*, 17531-17537.

(30) Markovic, N. M. P. N. R.; Ross, P. N., New electrocatalysts for fuel cells from model surfaces to commercial catalysts, *CATTECH,* **2000**, *4*, 110-126.
(31) Stamenkovic, V.; Mun Bongjin, S.; Mayrhofer Karl, J. J.; Ross Philip, N.; Markovic Nenad, M.; Rossmeisl, J.; Greeley, J.; Nørskov Jens, K., Changing the activity of electrocatalysts for oxygen reduction by tuning the surface electronic structure, *Angewandte Chemie,* **2006**, *118*, 2963-2967.
(32) Kyriakou, V.; Garagounis, I.; Vasileiou, E.; Vourros, A.; Stoukides, M., Progress in the electrochemical synthesis of ammonia, *Catalysis Today,* **2017**, *286*, 2-13.
(33) Hori, Y.; Wakebe, H.; Tsukamoto, T.; Koga, O., Electrocatalytic process of CO selectivity in electrochemical reduction of CO_2 at metal electrodes in aqueous media, *Electrochimica Acta,* **1994**, *39*, 1833-1839.
(34) Nie, X.; Luo, W.; Janik, M. J.; Asthagiri, A., Reaction mechanisms of CO_2 electrochemical reduction on Cu(111) determined with density functional theory, *J Catal,* **2014**, *312*, 108-122.
(35) Lim, R. J.; Xie, M. S.; Sk, M. A.; Lee, J. M.; Fisher, A.; Wang, X.; Lim, K. H., A review on the electrochemical reduction of CO_2 in fuel cells, metal electrodes and molecular catalysts, *Catalysis Today,* **2014**, *233*, 169-180.
(36) Zope, B. N.; Hibbitts, D. D.; Neurock, M.; Davis, R. J., Reactivity of the gold/water Interface during selective oxidation catalysis, *Science,* **2010**, *330*, 74-78.
(37) Taylor, C. D.; Neurock, M., Theoretical insights into the structure and reactivity of the aqueous/metal interface, *Current Opinion in Solid State and Materials Science,* **2005**, *9*, 49-65.
(38) Tomasi, J.; Persico, M., Molecular-interactions in solution - an overview of methods based on continuous distributions of the solvent, *Chemical Reviews,* **1994**, *94*, 2027-2094.
(39) Cramer, C. J.; Truhlar, D. G., Implicit solvation models: equilibria, structure, spectra, and dynamics, *Chemical Reviews,* **1999**, *99*, 2161-2200.
(40) Klamt, A., The COSMO and COSMO‐RS solvation models, *Wiley Interdisciplinary Reviews: Computational Molecular Science,* **2018**, *8*, e1338.
(41) te Velde, G.; Bickelhaupt, F. M.; Baerends, E. J.; Fonseca Guerra, C.; van Gisbergen, S. J. A.; Snijders, J. G.; Ziegler, T., Chemistry with ADF, *Journal of Computational Chemistry,* **2001**, *22*, 931-967.
(42) Jeong, K.-H.; Byun, B.-J.; Kang, Y.-K., Conformational preferences of glycerol in the gas phase and in water, *Bulletin of the Korean Chemical Society,* **2012**, *33*, 917-924.
(43) Fattebert, J. L.; Gygi, F., Density functional theory for efficient ab initio molecular dynamics simulations in solution, *Journal of Computational Chemistry,* **2002**, *23*, 662-666.
(44) Fattebert, J. L.; Gygi, F., First‐principles molecular dynamics simulations in a continuum solvent, *International Journal of Quantum Chemistry,* **2003**, *93*, 139-147.
(45) Petrosyan, S. A.; Rigos, A. A.; Arias, T. A., Joint density-functional theory: *Ab initio* study of Cr_2O_3 surface chemistry in solution, *Journal of Physical Chemistry B,* **2005**, *109*, 15436-15444.
(46) Fishman, M.; Zhuang, H. L.; Mathew, K.; Dirschka, W.; Hennig, R. G., Accuracy of exchange-correlation functionals and effect of solvation on the surface energy of copper, *Physical Review B,* **2013**, *87*, 245402.

(47) Mathew, K.; Sundararaman, R.; Letchworth-Weaver, K.; Arias, T. A.; Hennig, R. G., Implicit solvation model for density-functional study of nanocrystal surfaces and reaction pathways, *The Journal of Chemical Physics,* **2014**, *140*, 084106.
(48) Garcia-Ratés, M.; López, N., Multigrid-Based methodology for implicit solvation models in periodic DFT, *Journal of Chemical Theory and Computation,* **2016**, *12*, 1331-1341.
(49) Iyemperumal Satish, K.; Deskins, N. A., Evaluating Solvent Effects at the Aqueous/Pt(111) Interface, *ChemPhysChem,* **2017**, *18*, 2171-2190.
(50) William, L. J.; Jayaraman, C.; Jeffry, D. M.; Roger, W. I.; Michael, L. K., Comparison of simple potential functions for simulating liquid water, *The Journal of Chemical Physics,* **1983**, *79*, 926-935.
(51) Car, R.; Parrinello, M., Unified approach for molecular dynamics and density-functional theory, *Physical Review Letters,* **1985**, *55*, 2471-2474.
(52) Thiel, P. A.; Madey, T. E., The interaction of water with solid-surfaces - fundamental-aspects, *Surface Science Reports,* **1987**, *7*, 211-385.
(53) Ogasawara, H.; Brena, B.; Nordlund, D.; Nyberg, M.; Pelmenschikov, A.; Pettersson, L. G. M.; Nilsson, A., Structure and bonding of water on Pt(111), *Physical Review Letters,* **2002**, *89*, 276102.
(54) Ogasawara, H.; Yoshinobu, J.; Kawai, M., Water-adsorption on Pt(111) - from isolated molecule to 3-dimensional cluster, *Chemical Physics Letters,* **1994**, *231*, 188-192.
(55) Carrasco, J.; Hodgson, A.; Michaelides, A., A molecular perspective of water at metal interfaces, *Nature Materials,* **2012**, *11*, 667.
(56) Nie, S.; Feibelman, P. J.; Bartelt, N. C.; Thurmer, K., Pentagons and Heptagons in the First Water Layer on Pt(111), *Physical Review Letters,* **2010**, *105*.
(57) Feibelman, P. J.; Bartelt, N. C.; Nie, S.; Thurmer, K., Interpretation of high-resolution images of the best-bound wetting layers on Pt(111), *Journal of Chemical Physics,* **2010**, *133*.
(58) Feibelman, P. J., Partial Dissociation of Water on Ru(0001), *Science,* **2002**, *295*, 99.
(59) Forster, M.; Raval, R.; Hodgson, A.; Carrasco, J.; Michaelides, A., c(2 x 2) water-hydroxyl layer on Cu(110): a wetting layer stabilized by bjerrum defects, *Physical Review Letters,* **2011**, *106*, 046103.
(60) Schnur, S.; Groß, A., Properties of metal–water interfaces studied from first principles, *New Journal of Physics,* **2009**, *11*, 125003.
(61) Desai, S. K.; Neurock, M., First-principles study of the role of solvent in the dissociation of water over a Pt-Ru alloy, *Physical Review B,* **2003**, *68*, 075420.
(62) Peterson, A. A.; Abild-Pedersen, F.; Studt, F.; Rossmeisl, J.; Nørskov, J. K., How Copper Catalyzes the Electroreduction of Carbon Dioxide into Hydrocarbon Fuels, *Energy & Environmental Science,* **2010**, *3*, 1311-1315.
(63) Durand, W. J.; Peterson, A. A.; Studt, F.; Abild-Pedersen, F.; Nørskov, J. K., Structure Effects on the Energetics of the Electrochemical Reduction of CO_2 by Copper Surfaces, *Surface Science,* **2011**, *605*, 1354-1359.
(64) Peterson, A. A.; Nørskov, J. K., Activity Descriptors for CO_2 Electroreduction to Methane on Transition-Metal Catalysts, *Journal of Physical Chemistry Letters,* **2012**, *3*, 251-258.
(65) Shi, C.; Chan, K.; Yoo, J. S.; Nørskov, J. K., Barriers of Electrochemical CO_2 Reduction on Transition Metals, *Organic Process Research & Development,* **2016**, *20*, 1424-1430.
(66) Hussain, J.; Skúlason, E.; Jónsson, H., Computational Study of Electrochemical CO_2 Reduction at Transition Metal Electrodes, *Procedia Computer Science,* **2015**, *51*, 1865-1871.

(67) Skúlason, E.; Jónsson, H., Atomic Scale Simulations of Heterogeneous Electrocatalysis: Recent Advances, *Advances in Physics: X,* **2017**, *2*, 481-495.
(68) Nie, X.; Esopi, M. R.; Janik, M. J.; Asthagiri, A., Selectivity of CO_2 Reduction on Copper Electrodes: The Role of the Kinetics of Elementary Steps, *Angewandte Chemie International Edition,* **2013**, *52*, 2459-2462.
(69) Skulason, E.; Karlberg, G. S.; Rossmeisl, J.; Bligaard, T.; Greeley, J.; Jonsson, H.; Norskov, J. K., Density functional theory calculations for the hydrogen evolution reaction in an electrochemical double layer on the Pt(111) electrode, *Physical Chemistry Chemical Physics,* **2007**, *9*, 3241-3250.
(70) Skulason, E.; Tripkovic, V.; Bjorketun, M. E.; Gudmundsdottir, S.; Karlberg, G.; Rossmeisl, J.; Bligaard, T.; Jonsson, H.; Norskov, J. K., Modeling the electrochemical hydrogen oxidation and evolution reactions on the basis of density functional theory calculations, *Journal of Physical Chemistry C,* **2010**, *114*, 18182-18197.
(71) Hartnig, C.; Grimminger, J.; Spohr, E., Adsorption of Formic Acid on Pt(111) in the Presence of Water, *Journal of Electroanalytical Chemistry,* **2007**, *607*, 133-139.
(72) Zhang, Y.-C.; Ren, R.-P.; Liu, S.-Z.; Zuo, Z.-J.; Lv, Y.-K., Theoretical Study on the Influence of A Secondary Metal on the Cu(110) Surface in the Presence of H_2O for Methanol Decomposition, *RSC Advances,* **2016**, *6*, 15127-15136.
(73) Michel, C.; Auneau, F.; Delbecq, F.; Sautet, P., C–H versus O–H Bond Dissociation for Alcohols on a Rh(111) Surface: A Strong Assistance from Hydrogen Bonded Neighbors, *ACS Catalysis,* **2011**, *1*, 1430-1440.
(74) Garcia-Ratés, M.; García-Muelas, R.; López, N., Solvation effects on methanol decomposition on Pd(111), Pt(111), and Ru(0001), *The Journal of Physical Chemistry C,* **2017**, *121*, 13803-13809.
(75) Shustorovich, E., Activation Barrier for Adsorbate Surface Diffusion, Heat of Chemisorption, and Adsorbate Registry: Theoretical Interrelations, *Journal of the American Chemical Society,* **1984**, *106*, 6479-6481.
(76) Shustorovich, E.; Sellers, H., The UBI-QEP method: a practical theoretical approach to understanding chemistry on transition metal surfaces, *Surface Science Reports,* **1998**, *31*, 1-119.
(77) Kua, J.; Faglioni, F.; Goddard, W. A., Thermochemistry for hydrocarbon intermediates chemisorbed on metal surfaces: $CH_{n-m}(CH_3)_m$ with n=1, 2, 3 and $m \leqslant n$ on Pt, Ir, Os, Pd, Ph, and Ru, *Journal of the American Chemical Society,* **2000**, *122*, 2309-2321.
(78) Abild-Pedersen, F.; Greeley, J.; Studt, F.; Rossmeisl, J.; Munter, T. R.; Moses, P. G.; Skulason, E.; Bligaard, T.; Nørskov, J. K., Scaling properties of adsorption energies for hydrogen-containing molecules on transition-metal surfaces, *Physical Review Letters,* **2007**, *99*, 016105-016101.
(79) Bodenschatz, C. J.; Sarupria, S.; Getman, R. B., Molecular-Level Details about Liquid H_2O Interactions with CO and Sugar Alcohol Adsorbates on Pt(111) Calculated Using Density Functional Theory and Molecular Dynamics, *The Journal of Physical Chemistry C,* **2015**, *119*, 13642-13651.
(80) Xie, T.; Sarupria, S.; Getman, R. B., A DFT and MD Study of Aqueous-Phase Dehydrogenation of Glycerol on Pt(111): Comparing Chemical Accuracy Versus Computational Expense in Different Methods for Calculating Aqueous-Phase System Energies, *Molecular Simulation,* **2017**, *43*, 370-378.

(81) Kresse, G.; Hafner, J., Ab *initio* molecular dynamics for open shell transition metals, *Physical Review B,* **1993**, *48*, 13115-13118.
(82) Kresse, G.; Furthmuller, J., Efficiency of *Ab initio* Total Energy Calculations for Metals and Semiconductors using A Plane-wave Basis Set, *Computational Materials Science,* **1996**, *6*, 15-50.
(83) Monkhorst, H. J.; Pack, J. D., Special Points for Brillouin Zone Integrations, *Physical Review B,* **1976**, *13*, 5188-5192.
(84) Kiran, M.; Ravishankar, S.; Kendra, L.-W.; Arias, T. A.; Richard, G. H., Implicit solvation model for density-functional study of nanocrystal surfaces and reaction pathways, *The Journal of Chemical Physics,* **2014**, *140*, 084106.
(85) Tereshchuk, P.; Da Silva, J. L. F., Density functional investigation of the adsorption of ethanol–water mixture on the Pt(111) surface, *The Journal of Physical Chemistry C,* **2013**, *117*, 16942-16952.
(86) Tereshchuk, P.; Chaves, A. S.; Da Silva, J. L. F., Glycerol adsorption on platinum surfaces: a density functional theory investigation with van der waals corrections, *The Journal of Physical Chemistry C,* **2014**, *118*, 15251-15259.
(87) Fernández, P. S.; Fernandes Gomes, J.; Angelucci, C. A.; Tereshchuk, P.; Martins, C. A.; Camara, G. A.; Martins, M. a. E.; Da Silva, J. L. F.; Tremiliosi-Filho, G., Establishing a link between well-ordered Pt(100) surfaces and real systems: how do random superficial defects influence the electro-oxidation of glycerol?, *ACS Catalysis,* **2015**, *5*, 4227-4236.
(88) Fernández, P. S.; Tereshchuk, P.; Angelucci, C. A.; Gomes, J. F.; Garcia, A. C.; Martins, C. A.; Camara, G. A.; Martins, M. a. E.; Da Silva, J. L. F.; Tremiliosi-Filho, G., How do random superficial defects influence the electro-oxidation of glycerol on Pt(111) surfaces?, *Physical Chemistry Chemical Physics,* **2016**, *18*, 25582-25591.
(89) Amaral, R. C.; Tereshchuk, P.; Seminovski, Y.; Da Silva, J. L. F., The role of low-coordinated sites on the adsorption of glycerol on defected Pt_n/Pt(111) substrates: a density functional investigation within the D3 van der waals correction, *The Journal of Physical Chemistry C,* **2017**, *121*, 3445-3454.
(90) Tereshchuk, P.; Amaral, R. C.; Seminovski, Y.; Da Silva, J. L. F., Glycerol adsorption on a defected Pt_6/Pt(100) substrate: a density functional theory investigation within the D3 van der Waals correction, *RSC Advances,* **2017**, *7*, 17122-17127.
(91) Phatak, A. A.; Delgass, W. N.; Ribeiro, F. H.; Schneider, W. F., Density functional theory comparison of water dissociation steps on Cu, Au, Ni, Pd, and Pt, *The Journal of Physical Chemistry C,* **2009**, *113*, 7269-7276.
(92) Zhou, M.; Liu, B., DFT investigation on the competition of the water–gas shift reaction versus methanation on clean and potassium‐modified nickel(1 1 1) surfaces, *Chemcatchem,* **2015**, *7*, 3928-3935.
(93) Michaelides, A., Density Functional Theory Simulations of Water–Metal Interfaces: Waltzing Waters, A Novel 2d Ice Phase, and More, *Applied Physics A,* **2006**, *85*, 415-425.
(94) Tereshchuk, P.; Da Silva, J. L. F., Ethanol and water adsorption on close-packed 3d, 4d, and 5d transition-metal surfaces: a density functional theory Investigation with van der Waals correction, *The Journal of Physical Chemistry C,* **2012**, *116*, 24695-24705.
(95) Heras, J. M.; Viscido, L., Work function changes upon water contamination of metal surfaces, *Applications of Surface Science,* **1980**, *4*, 238-241.

(96) Filhol, J. S.; Bocquet, M. L., Charge control of the water monolayer/Pd interface, *Chemical Physics Letters,* **2007**, *438*, 203-207.
(97) Crotti, C.; Kaspar, J.; Farnetti, E., Dehydrogenation of glycerol to dihydroxyacetone catalyzed by iridium complexes with P-N ligands, *Green Chemistry,* **2010**, *12*, 1295-1300.
(98) Hakim, S. S. M. A.; S., T. A.; Kenichi, K.; Takashi, T.; Ken‐ichi, S., Oxidant‐free Dehydrogenation of Glycerol to Lactic Acid by Heterogeneous Platinum Catalysts, *Chemcatchem,* **2017**, *9*, 2816-2821.
(99) Groß, A.; Gossenberger, F.; Lin, X.; Naderian, M.; Sakong, S.; Roman, T., Water structures at metal electrodes studied by *ab initio* molecular dynamics simulations, *Journal of the Elecrochemical Society,* **2014**, *161*, E3015-E3020.
(100) Spohr, E., Computer-simulation of the water platinum interface, *Journal of Physical Chemistry,* **1989**, *93*, 6171-6180.
(101) Spohr, E., Effect of electrostatic boundary conditions and system size on the interfacial properties of water and aqueous solutions, *Journal of Chemical Physics,* **1997**, *107*, 6342-6348.
(102) Raghavan, K.; Foster, K.; Motakabbir, K.; Berkowitz, M., Structure and dynamics of water at the Pt(111) interface: Molecular dynamics study, *The Journal of Chemical Physics,* **1991**, *94*, 2110-2117.
(103) Xia, X.; Berkowitz, M. L., Electric-field induced restructuring of water at a platinum-water interface: A molecular dynamics computer simulation, *Physical Review Letters,* **1995**, *74*, 3193-3196.
(104) Sergei, I.; Alain, M.; Kirk, V.; Gregory, A. V., Ab initio molecular dynamics simulation of the Cu(110)–water interface, *The Journal of Chemical Physics,* **2001**, *114*, 3248-3257.
(105) Shan, N.; Hanchett, M. K.; Liu, B., Mechanistic insights evaluating Ag, Pb, and Ni as electrocatalysts for furfural reduction from first-principles methods, *Journal of Physical Chemistry C,* **2017**, *121*, 25768-25777.
(106) Shan, N.; Zhou, M.; Hanchett, M. K.; Chen, J.; Liu, B., Practical Principles of Density Functional Theory for Catalytic Reaction Simulations on Metal Surfaces – from Theory to Applications, *Molecular Simulation,* **2017**, *43*, 861-885.
(107) Rossmeisl, J.; Skúlason, E.; Björketun, M. E.; Tripkovic, V.; Nørskov, J. K., Modeling the electrified solid–liquid interface, *Chemical Physics Letters,* **2008**, *466*, 68-71.

TOC

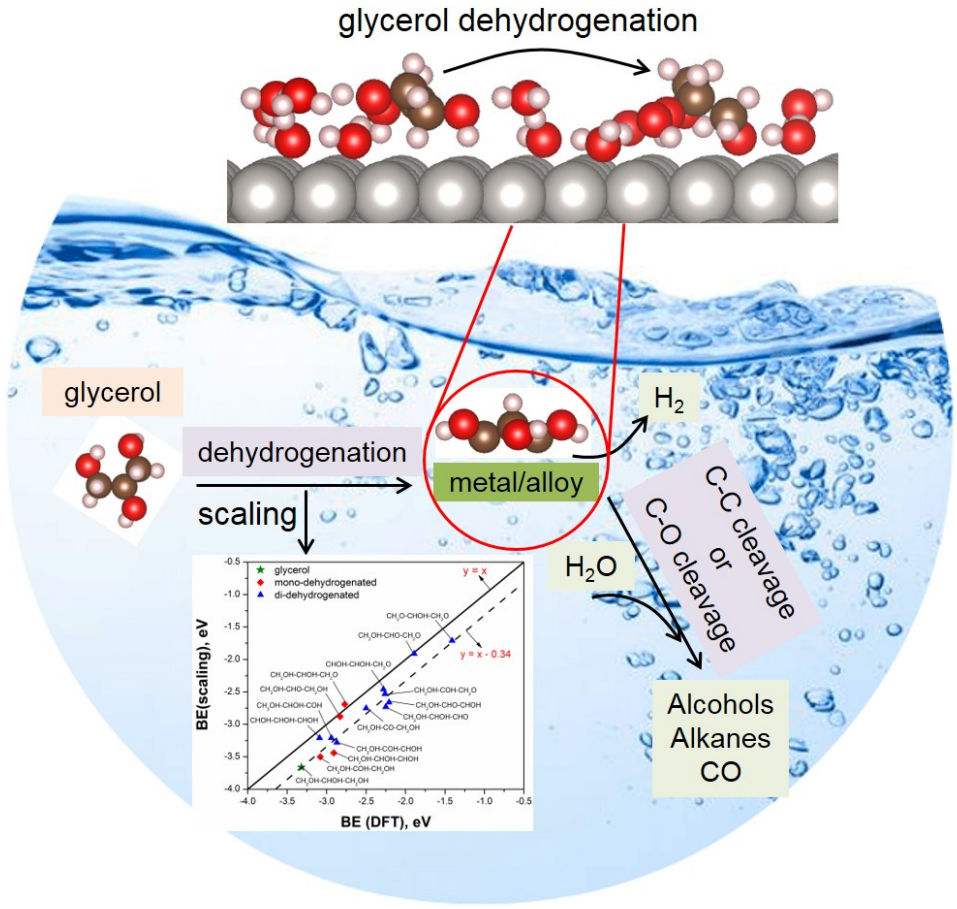
glycerol dehydrogenation
glycerol
dehydrogenation
scaling
metal/alloy
H_2
H_2O
C-C cleavage
or
C-O cleavage
Alcohols
Alkanes
CO
glycerol
mono-dehydrogenated
di-dehydrogenated
y = x
y = x - 0.34
BE(scaling), eV
BE (DFT), eV

Biographies

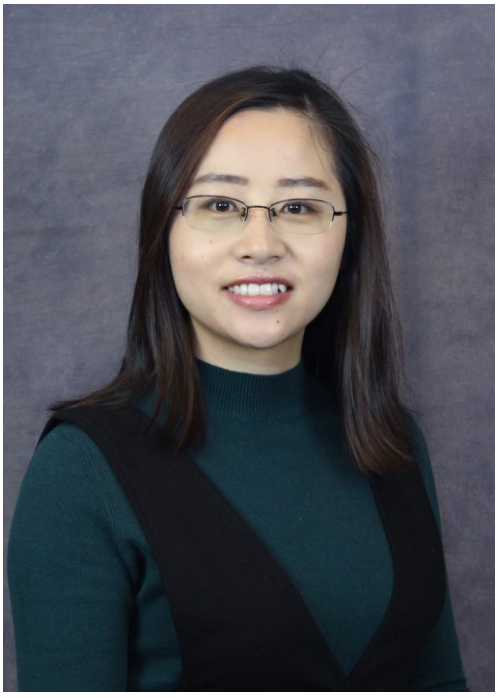

Nannan Shan is a Ph.D. candidate in chemical engineering at Kansas State University. She received her M.Sc. in chemical engineering and technology (2013) from Beijing University of Chemical Technology and her B.Sc. degree in applied chemistry (2010) from Qingdao Agricultural University. Her research interest is in sustainable chemicals and fuels productions via both electrochemical and thermochemical approaches using density functional theory.

Bin Liu is an assistant professor in the Department of Chemical Engineering at Kansas State

University. Bin Liu received his B.S. in Chemical Engineering from Dalian University of Technology in China in 2003, and Ph.D. degree in Chemical Engineering from Colorado School of Mines in 2008. Bin Liu also worked as a postdoctoral researcher at the Center for Nanoscale Materials of Argonne National Laboratory. His research interests include surface chemistry, heterogeneous catalysis, electrochemistry, novel technologies related to fuels and chemicals productions, and materials engineering, using quantum mechanical calculations.